NAVAL POSTGRADUATE SCHOOL

MONTEREY, CALIFORNIA

THESIS

CLIMATOLOGICAL VARIABILITY OF MICROWAVE DUCTING IN THE SOUTHERN CALIFORNIA REGION

by

Dian N. Candelario

September 2023

Thesis Advisor: Qing Wang
Co-Advisor: Paul A. Frederickson

THIS PAGE INTENTIONALLY LEFT BLANK

REPORT DOCUMENTATION PAGE	*Form Approved OMB No. 0704-0188*

1. AGENCY USE ONLY *(Leave blank)*	**2. REPORT DATE** September 2023	**3. REPORT TYPE AND DATES COVERED** Master's thesis

4. TITLE AND SUBTITLE
CLIMATOLOGICAL VARIABILITY OF MICROWAVE DUCTING IN THE SOUTHERN CALIFORNIA REGION

5. FUNDING NUMBERS

6. AUTHOR(S) Dian N. Candelario

7. PERFORMING ORGANIZATION NAME(S) AND ADDRESS(ES)
Naval Postgraduate School
Monterey, CA 93943-5000

8. PERFORMING ORGANIZATION REPORT NUMBER

9. SPONSORING / MONITORING AGENCY NAME(S) AND ADDRESS(ES)
N/A

10. SPONSORING / MONITORING AGENCY REPORT NUMBER

11. SUPPLEMENTARY NOTES The views expressed in this thesis are those of the author and do not reflect the official policy or position of the Department of Defense or the U.S. Government.

12a. DISTRIBUTION / AVAILABILITY STATEMENT
Approved for public release. Distribution is unlimited.

12b. DISTRIBUTION CODE
A

13. ABSTRACT (maximum 200 words)

The Department of Defense (DOD) utilizes electromagnetic (EM) waves for communication, radar detection, and weapon guidance systems. It is hence crucial to understand the regional climatological characteristics of the atmosphere that significantly impact EM signal propagation. There are two major objectives of this thesis work. One is to evaluate the European Centre for Medium-Range Weather Forecasts (ECMWF) latest reanalysis product, the ECMWF Re-Analysis V5 (ERA5) dataset for identifying trapping conditions in the coastal marine environment. The other is to examine the climatology of ducting conditions in the southern California bights using the ERA5 data. To accomplish the first objective, we used the ERA5 measurements near the Sea Range at Point Mugu during a past field campaign. We then analyzed nine years of the ERA5 data in the Point Mugu area to determine any climatological differences in the trapping conditions between the years. We found that the ERA5 approximates well trapping conditions in the southern California bights area and discovered seasonal trends of the ducting characteristics as well as their spatial variations.

14. SUBJECT TERMS electromagnetic wave propagation, climatology, ducting	**15. NUMBER OF PAGES** 63
	16. PRICE CODE

17. SECURITY CLASSIFICATION OF REPORT	**18. SECURITY CLASSIFICATION OF THIS PAGE**	**19. SECURITY CLASSIFICATION OF ABSTRACT**	**20. LIMITATION OF ABSTRACT**
Unclassified	Unclassified	Unclassified	UU

NSN 7540-01-280-5500

Standard Form 298 (Rev. 2-89)
Prescribed by ANSI Std. 239-18

THIS PAGE INTENTIONALLY LEFT BLANK

Approved for public release. Distribution is unlimited.

CLIMATOLOGICAL VARIABILITY OF MICROWAVE DUCTING IN THE SOUTHERN CALIFORNIA REGION

Dian N. Candelario
First Lieutenant, United States Air Force
BS, University of South Alabama, 2021

Submitted in partial fulfillment of the
requirements for the degree of

MASTER OF SCIENCE IN METEOROLOGY

from the

NAVAL POSTGRADUATE SCHOOL
September 2023

Approved by: Qing Wang
Advisor

Paul A. Frederickson
Co-Advisor

Wendell A. Nuss
Chair, Department of Meteorology

THIS PAGE INTENTIONALLY LEFT BLANK

ABSTRACT

The Department of Defense (DOD) utilizes electromagnetic (EM) waves for communication, radar detection, and weapon guidance systems. It is hence crucial to understand the regional climatological characteristics of the atmosphere that significantly impact EM signal propagation. There are two major objectives of this thesis work. One is to evaluate the European Centre for Medium-Range Weather Forecasts (ECMWF) latest reanalysis product, the ECMWF Re-Analysis V5 (ERA5) dataset for identifying trapping conditions in the coastal marine environment. The other is to examine the climatology of ducting conditions in the southern California bights using the ERA5 data. To accomplish the first objective, we used the ERA5 measurements near the Sea Range at Point Mugu during a past field campaign. We then analyzed nine years of the ERA5 data in the Point Mugu area to determine any climatological differences in the trapping conditions between the years. We found that the ERA5 approximates well trapping conditions in the southern California bights area and discovered seasonal trends of the ducting characteristics as well as their spatial variations.

THIS PAGE INTENTIONALLY LEFT BLANK

TABLE OF CONTENTS

THIS PAGE INTENTIONALLY LEFT BLANK

LIST OF FIGURES

LIST OF TABLES

THIS PAGE INTENTIONALLY LEFT BLANK

LIST OF ACRONYMS AND ABBREVIATIONS

AFDP	Air Force Doctrine Publication
ASTD	average surface temperature difference
CASPER	Coupled Air-Sea Processes and Electromagnetic wave ducting Research
DJF	December, January, February
DOD	Department of Defense
ECMWF	European Centre for Medium-Range Weather Forecasts
EM	electromagnetic
EMS	electromagnetic spectrum
EMSO	electromagnetic spectrum operations
ERA5	ECMWF Re-Analysis V5
FLIP	Floating Instrument Platform
FLIPI	interpolated FLIP
IPCC	Intergovernmental Panel on Climate Change
JJA	June, July, August
MABL	marine atmospheric boundary layer
MAM	March, April, May
MASL	marine atmospheric surface layer
NE	Northeast
OE	operational environment
RVSR	Research Vessel *Sally Ride*
RVSRI	interpolated RVSR
SON	September, October, November
SW	Southwest

THIS PAGE INTENTIONALLY LEFT BLANK

ACKNOWLEDGMENTS

I'd like to first thank Professor Qing Wang for her endless support and helpfulness during the journey. She was able to answer questions and guide me through this thesis even with her busy schedule and numerous trips overseas. I am also thankful to Mr. Paul Frederickson for his invaluable help and guidance. He was always there when I had a MATLAB question or a question regarding the ERA5 model data set. Thanks as well to the Naval Postgraduate School Meteorology Department as all the professors there were there to help from start to finish.

A big thank you to my hardworking and wonderful wife, Kaitlyn. Whether it was encouraging me to press on, watching our son while I worked, or any number of other amazing things she did to allow me to finish, I am so grateful to her and none of this would have been possible without her.

THIS PAGE INTENTIONALLY LEFT BLANK

I. INTRODUCTION

A. CONTEXT

According to the Air Force Doctrine Publication (AFDP) 3–51, "Electromagnetic Warfare and Electromagnetic Spectrum Operations," "Electromagnetic spectrum operations (EMSO) comprise all coordinated military actions to exploit, attack, protect, and manage the electromagnetic (EM) environment to achieve the commander's objectives" (LeMay Center for Doctrine, 2019). The doctrine also goes on to say that one's military must protect "spectrum-dependent systems, networks and operations; tactically sensing the operational environment (OE); and attacking where necessary, at a time and place of their choice." in order to "obtain and maintain situational mastery of the electromagnetic spectrum (EMS)" (LeMay Center for Doctrine, 2019). To achieve that, one must understand how the EMS is impacted by atmospheric conditions, and how to exploit knowledge of current and future weather conditions to achieve EMS superiority against our adversaries.

Climatology is a major factor that affects EM propagation. The Intergovernmental Panel on Climate Change (IPCC) 6th report predicts that mean atmospheric temperatures will warm from 1.5°C to 3.0°C within the next century, which will have implications on how electromagnetic waves propagate in the atmosphere (Pörtner, H.-O. et al. 2022). Different climates have different effects on EM propagation, due to varying changes in temperature, moisture, and pressure in different regions of the globe. To gain insight into the current and predicted future state of the global climate, it is important to examine climate changes that have occurred in the recent past, which is a main focus of this work.

B. IMPORTANCE OF ACCURATE FORECAST OF THE EM PROPAGATION CONDITIONS

Accurate forecasts for EM propagation conditions are crucial to many aspects of conducting operations within the Department of Defense (DOD). For example, the radar detection of airborne and surface platforms can be strongly impacted by varying atmospheric conditions, therefore accurate atmospheric forecasts can lead to improved

detection of an adversary's platforms, while also enabling our own assets to elude detection. Some of our weapons systems, such as radar-guided missiles, can also exploit accurate forecasts of EM propagation conditions to better detect, track and home-in on their targets. Communications are impacted the most by accurate forecasts for EM propagation condition. Radio and cellphone communications utilize these ducting and trapping layers to get their signals further out so knowing the locations of these ducts and trapping layers is key for smooth execution of operations. Exploiting weather forecasts to improve EMS operations within microwave frequencies depends in large part on accurately predicting the location, timing and attributes of atmospheric ducts and trapping layers, which will be discussed in the next section.

C. OBJECTIVES OF THESIS WORK

There are two major objectives of this thesis work. One is to evaluate the latest European Centre for Medium-Range Weather Forecasts (ECMWF) reanalysis product, the ECMWF Re-Analysis V5 (ERA5) dataset, to gain a better understanding of its skill in predicting EM trapping conditions in the coastal marine environment. The other is to examine the climatology of ducting conditions in the southern California bights to better understand how they have changed in recent years and to gain insight into expected EM propagation conditions in the near future. To accomplish the first objective, we will compare atmospheric measurements obtained near the Sea Range at Point Mugu during a recent field campaign with ERA5 EM ducting predictions to determine their accuracy. We will then analyze nine years of ERA5 data in the Point Mugu area to determine any climatological changes in trapping conditions that may have occurred during that time period. Similar analyses can be done for other regions in future work.

This thesis is organized as follows: First we describe how EM waves propagate in the atmosphere, with a focus on ducting conditions that significantly impact radar detection of targets at microwave frequencies. The various ducting types are introduced in this section. Next, the reasons for choosing the ERA5 reanalysis data for this study will be explained, and the field measurements used for this study from the Coupled Air-Sea Processes and Electromagnetic wave ducting Research (CASPER) campaign will be

introduced in Chapter II. The methodology and results of using the CASPER project data to evaluate the accuracy of ERA5 predictions of trapping layer and ducts will be described in Chapter III. The use of ERA5 data to develop a climatology of EM ducting conditions for the southern California area will be presented in Chapter IV. Finally, the summary and conclusions of this work are presented in Chapter V.

THIS PAGE INTENTIONALLY LEFT BLANK

II. BACKGROUND

A. EM PROPAGATION IN THE ATMOSPHERE

EM waves propagating through the atmosphere are substantially affected by the atmospheric conditions, as described by the vertical gradient of the index of refraction. The index of refraction (n) is defined as the ratio of the speed of EM waves propagating through a medium over that in a vacuum, and can be expressed in terms of the atmospheric state variables of absolute temperature (T), partial pressure of water vapor (e) and total air pressure (p), as follows (Bean and Dutton 1968):

$$N = \left(\frac{77.6}{T}\right)\left(p + \frac{4810e}{T}\right) \tag{1.1}$$

The modified refractivity, M, is a dimensionless quantity that is often used to take into account the impact of the earth's curvature on EM propagation, and to facilitate the identification of atmospheric trapping layers:

$$M = N + 0.157z \tag{1.2}$$

where z (m) is the height above sea level. The impact of the atmosphere on refracting propagating EM waves can be categorized into four categories, based on the vertical gradient of M ($\mathrm{d}M/\mathrm{d}z$), as illustrated in Figure 1.

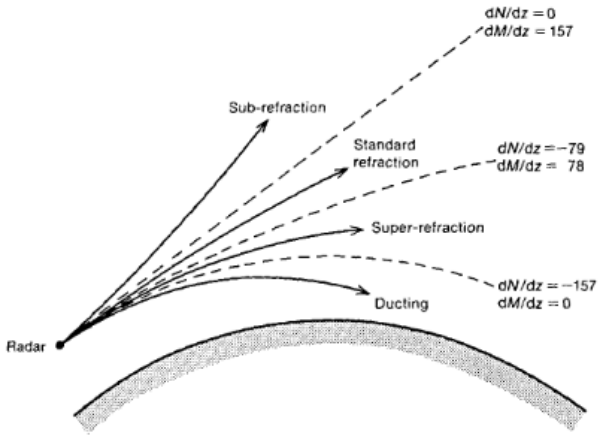

Sub-refraction, standard refraction, super-refraction, and ducting are shown. Values for the vertical gradient of refractivity (N) and modified refractivity (M) are given for the boundaries between the different refractive categories.

Figure 1. Different ray-paths showing the effects of atmospheric refractive conditions Source: Turton et al. (1988).

These four categories are standard refraction, sub-refraction, super-refraction, and ducting and they are determined by the current state of the atmosphere. The vertical gradient of M for a "standard atmosphere," defined as a global mean of atmospheric conditions in the troposphere, has a value of 117. Standard refraction occurs when dM/dz is between 157 and 78, and super-refraction occurs when dM/dz is between 78 and 0. Both of these cases denote a situation in which the propagating EM rays have a curvature less than the curvature of the Earth. Sub-refraction occurs when dM/dz is greater than 157, indicating a generally uncommon situation in which the propagating EM rays curve away from the Earth's surface. Sub-refraction near the surface is caused by warm, moist air occurring over a cooler surface. Ducting occurs when dM/dz is less than 0, indicating that the propagating EM rays have a curvature greater than the Earth's surface. Atmospheric layers with dM/dz less than 0 are referred to as 'trapping layers'. Trapping layers are most commonly caused by a rapid decrease in humidity with height within an atmospheric layer. Elevated trapping layers are often associated with temperature inversions as well. Ducts and their associated trapping layers are of special interest, because they can lead to greatly

extended radar detection and radio communications ranges, and for this reason, they are the focus of this thesis.

Figure 2 shows that ducts and trapping layers are easily identifiable when analyzing a vertical profile of the modified reflectivity. The location of the trapping layer within a profile determines whether the duct is a surface duct (a), surface-based duct (b), or an elevated duct (c). Surface ducts are formed by, and are coincident with, surface-based trapping layers. Surface-based ducts are formed by elevated trapping layers, when the top of the trapping layer has an *M* value less than the surface value. Elevated ducts are formed by elevated trapping layers, when the top of the trapping layer has an *M* value greater than the surface value. Elevated ducts are defined as the vertical region from the top of the trapping layer and ends at the height below the trapping layer where the *M* value of the profile is equal to the value at the top of the trapping layer.

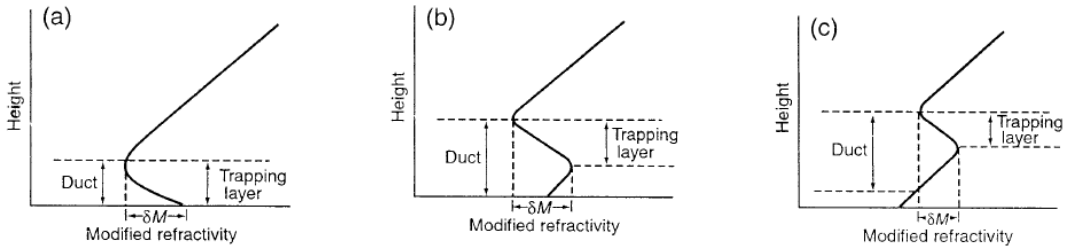

Figure 2. Surface ducts (a), surface-based ducts (b), and elevated ducts (c) shown here, as defined by the vertical gradient of *M* (d*M*/d*z*) Source: Turton et al. (1988).

B. ERA5 REANALYSES

To accomplish our goal of analyzing the climatology of ducting conditions in the southern California coastal region, we utilized the ECMWF's ERA5 global reanalysis data set. According to Hersbach et. al. (2020), ERA5 is the latest reanalysis from the ECMWF, which covers the time period from 1950 to the present day. ERA5 has 137 vertical levels from the surface to 1 Pa altitude and a horizontal grid resolution of 31 km at the equator. In this study we utilize the three-dimensional fields of temperature, humidity, and pressure from ERA5 to identify RF duct heights and strength at any particular grid point. Studies

like von Engel and Teixeria (2004) and Lopez (2009) utilizing older versions of the ECMWF data set, the ERA-40 and ERA-Interim, show that it is viable to use the data sets to get an accurate representation of an area with certain parameterizations, such as fitting the ERA-40 to a vertical grid with a 20 m resolution and removing topographic effects (von Engel and Teixeria 2004). The ERA5 has a higher vertical and horizontal resolution than the previous ECMWF reanalysis datasets, but the vertical profile data still need to be interpolated, which is discussed in the next section.

III. DATA AND METHODS

A. CASPER PROJECT

The CASPER project had four main objectives:

- to obtain a comprehensive and cohesive dataset to support in-depth analyses and modeling studies to address critical issues in air-sea interaction processes related to EM propagation
- to improve [marine atmospheric surface layer] (MASL) models in representing temperature and water vapor profiles in heterogeneous environments and under the effects of waves/swell
- to understand physical processes governing the properties of the inversion layer atop the [marine atmospheric boundary layer] (MABL) and improve their representation in EM propagation models
- to explore new approaches in EM modeling to represent the impact of the atmospheric environment with spatial and temporal variability (Wang et al. 2018)

The CASPER project consisted of two separate field campaigns, one that took place off the U.S. East Coast in 2015, and one that occurred off the West Coast in the fall of 2017, known as CASPER-West. This thesis only uses data collected during CASPER-West, which took place off the coast of Point Magu, California, from 27 September to 26 October 2017. During CASPER-West, environment measurements were obtained within and above the MABL, concurrently with EM propagation measurements within the lower atmosphere. To accomplish this, CASPER-West utilized the Floating Instrument Platform (FLIP), the Research Vessel *Sally Ride* (RVSR), a Twin Otter research aircraft, three buoys, and seven sea-going unmanned surface vehicles (Wang et al. 2019). The FLIP platform was located about 46.7 km south of Point Mugu and hosted a number of instruments that measured meteorological data. The RVSR had multiple instruments similar to the FLIP but it transited between the FLIP and Point Mugu. Multiple radiosonde launches were performed from both the FLIP and RVSR. These sounding data provided vertical profiles of modified refractivity, which revealed the current ducting conditions. A total of 400 radiosonde profiles were collected during the CASPER-West campaign, 217 obtained from the RVSR ship, and 183 obtained from the FLIP platform. These profiles

are used to evaluate the ability of the ERA5 data to identify ducting layers in the coastal environment.

The upper-air ducting conditions observed by the FLIP and RVSR radiosondes during the CASPER-West campaign are summarized in Figure 3. These time series plots show the duct top height, duct base height, and trapping layer base height for the strongest duct present in each profile obtained from the FLIP and RVSR platforms. Cases which have both the duct base and the trapping-layer base located at the surface denotes the occurrence of a surface duct. Cases with the trapping-layer base located above the surface and the duct base at the surface indicates the occurrence of a surface-based duct. When the duct base is located above the surface an elevated duct is present. In addition to indicating the upper-air duct types occurring in the profile, this figure also provides information on the height and thickness of the strongest ducts and trapping layers present in the profiles

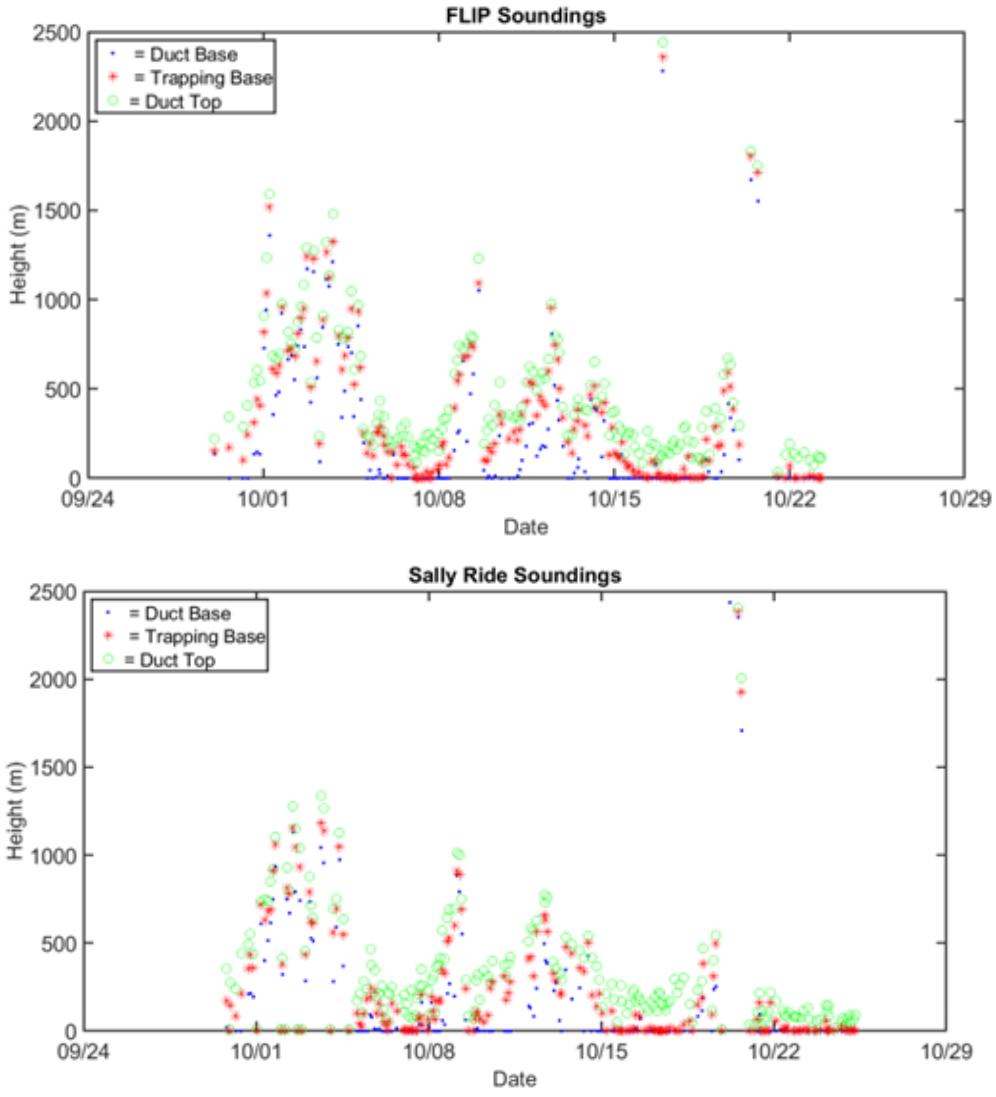

The strongest ducts identified from radiosonde profiles and the vertical axis is the height above the ocean surface.

Figure 3. The heights of the duct base (blue), duct top (green), and trapping layer base (red) from the FLIP and RVSR radiosonde profiles during CASPER-West.

B. PRE-PROCESSING OF CASPER SOUNDING DATA

The ERA5 reanalysis and the radiosonde data have very different vertical resolutions. Our initial effort in this work is to pre-process both datasets to ensure they have the same vertical resolution and height levels for duct detection and comparisons

between the radiosonde and ERA5 profiles. Figure 4 shows a comparison of the M-profiles from one of the RVSR radiosondes during CASPER-West and the corresponding ERA5 profile taken from the closest grid point and hour. The radiosonde data was recorded at 1 Hz, giving an average vertical resolution of about 3–5m, while the original ERA5 data had much coarser vertical resolution, varying from about 20 m near the surface to about 200 m at a height of 2500 m, which roughly corresponds to the highest duct top observed during CASPER-West (see Figure 3). The original ERA5 data points are shown by blue squares in Figure 4. This coarse resolution profile data was interpolated to 10-m vertical resolution, shown by the red dots. This finer resolution interpolated profile closely resembles the original ERA5 profile, but provides better-defined duct heights, thicknesses and strengths. The radiosonde data with much higher vertical resolution exhibits finer details and higher vertical variability in the modified refractivity, which are not represented in the ERA5 original or interpolated profiles. To make the duct layers identified from both data sources comparable, we first interpolate the sounding data onto the vertical grid of the ERA5 profile (shown as the pink squares). We then interpolated the resultant coarse-resolution profile into 10-m vertical resolution, as was done when processing the ERA5 profile (blue dots).

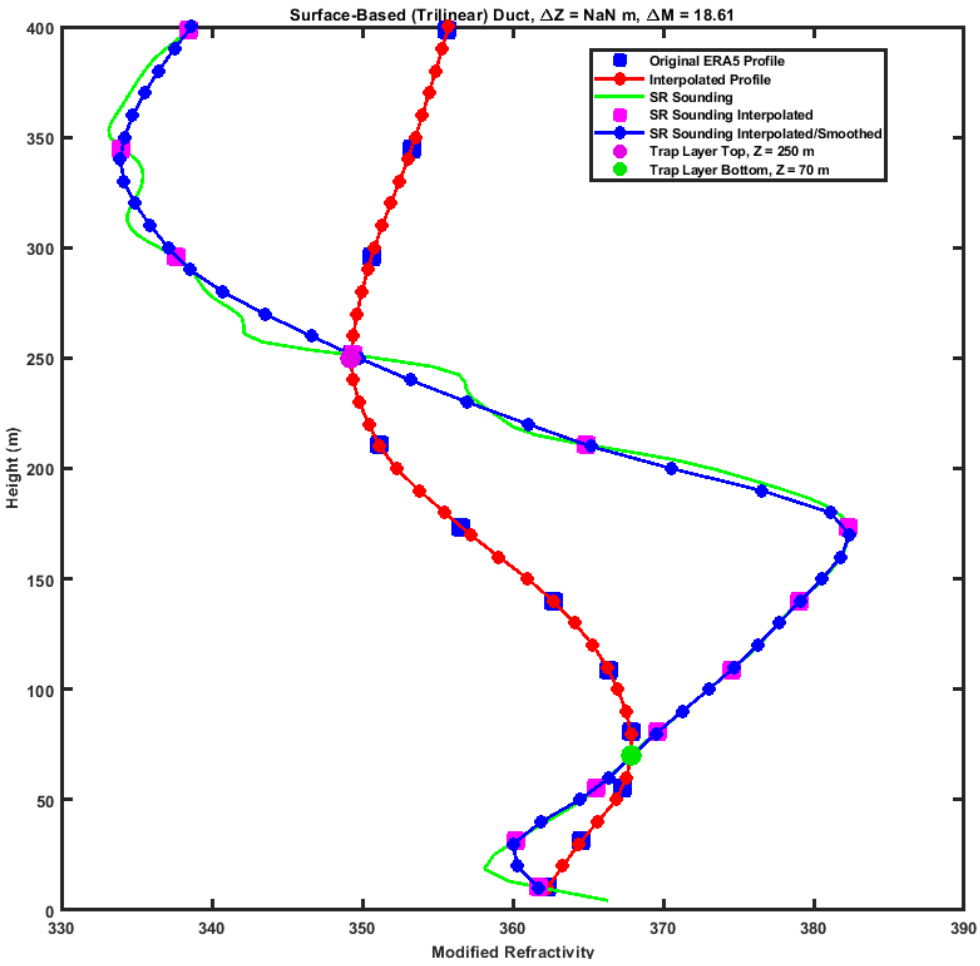

The red line is the ERA5 profile, the green line is the original RVSR profile, and the blue line is the interpolated/smoothed RVSR profile. The trapping layer base and top are also identified here.

Figure 4. A comparison between the ERA5 profile and a RVSR profile.

The impact of the pre-processing of the sounding data for identifying duct properties is evaluated and the results are shown in Figures 5–6 and Tables 1–2. In both of these figures, the duct properties from the original sounding data are compared with the corresponding interpolated profiles.

Figure 5 shows the comparison between the FLIP soundings and the interpolated FLIP (FLIPI) soundings. Figure 6 is broken up into sub-plots showing the comparisons of the heights of the duct top (a), duct base (b), trapping layer base (c), and the strength of the duct (d). The mean differences and absolute mean differences shown in Table 1 show that

the absolute mean difference for the heights vary between 20 and 25 meters, while the absolute mean difference for the duct strength is only 3 M-units. Both Figure 5 and Table 1 demonstrate that the main ducting features are well preserved through the interpolation, with mostly only small deviations from the original observed duct attributes, except for a small number of outlier points.

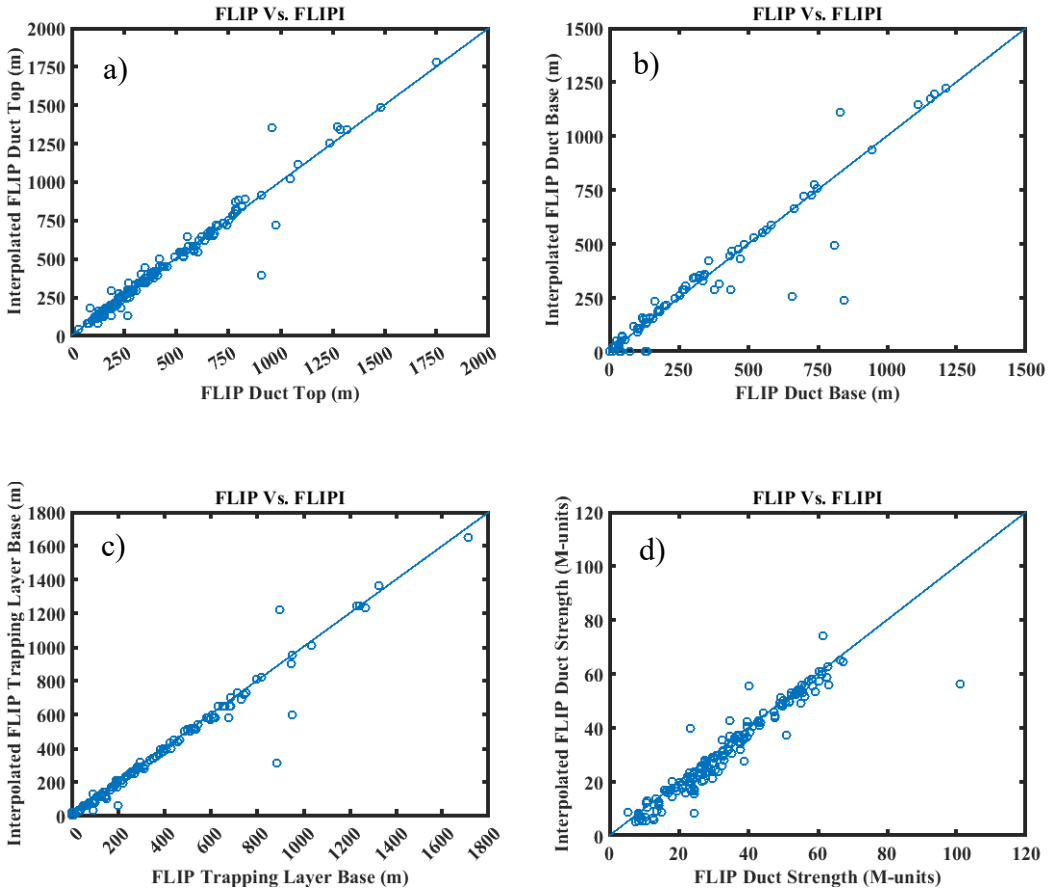

The heights of the duct tops (a), duct bases (b), and the trapping layer bases (c) are shown as well as the duct strengths (d)

Figure 5. Characteristics of the original FLIP soundings against the FLIPI soundings.

Table 1. Mean difference, absolute mean difference, and root mean square error between the FLIP soundings and the FLIPI soundings of the duct top, duct base, trapping layer base, and duct strength.

	Mean Difference	Absolute Mean Difference	Root Mean Square Error
Duct Top	-3.643 m	25.780 m	58.612
Duct Base	6.748 m	21.540 m	67.262
Trapping Layer Base	11.891 m	20.210 m	58.691
Duct Strength	2.193 M-units	3.138 M-units	5.158

Similar to the FLIP data, the interpolated RVSR (RVSRI) soundings show minimal deviation from the original RVSR soundings, except for a small number of outlier points. Figure 6 shows the same sub-plots for the different characteristics as were shown for the FLIP location. Minimal spread in the plots as well as low absolute mean difference from Table 2 show that the main duct features are preserved between the RVSR soundings and the RVSRI soundings.

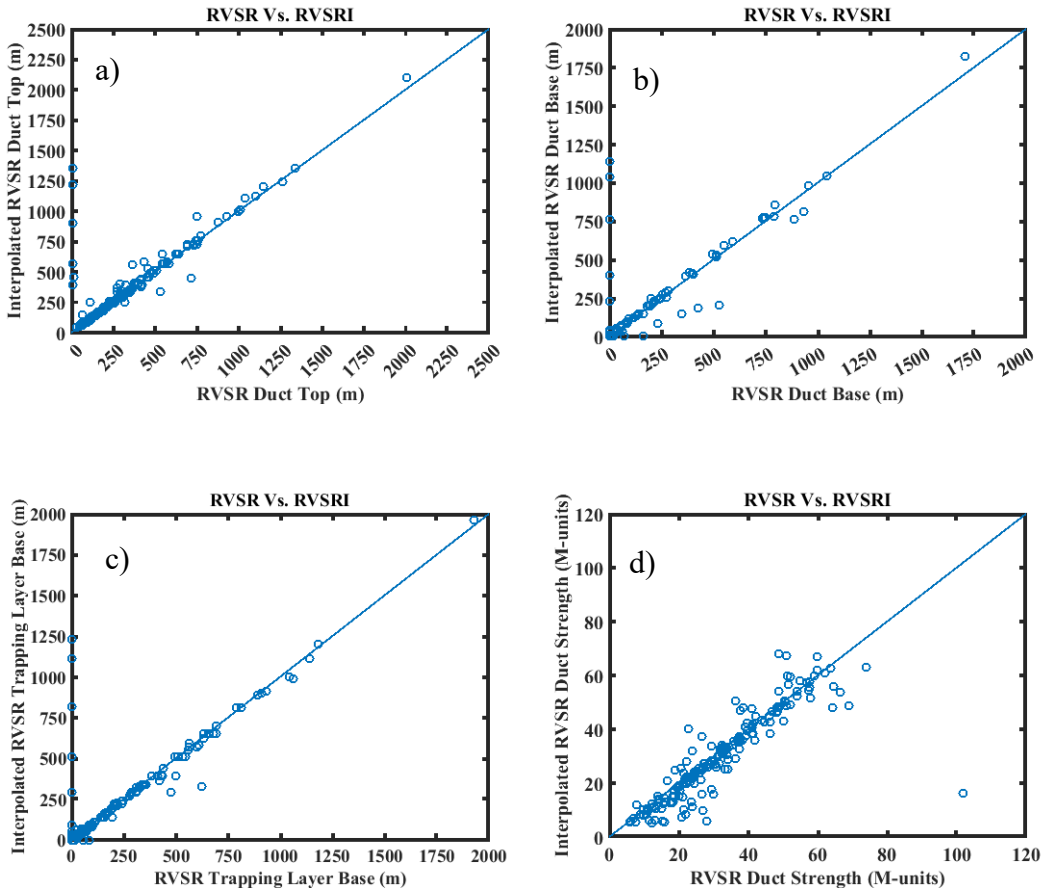

The heights of the duct tops (a), duct bases (b), and the trapping layer bases (c) are shown as well as the duct strengths (d).

Figure 6. Characteristics of the original RVSR soundings against the RVSRI soundings.

Table 2. Mean difference, absolute mean difference, and root mean square error between the RVSR soundings and the RVSRI soundings of the duct top, duct base, trapping layer base, and duct strength.

	Mean Difference	Absolute Mean Difference	Root Mean Square Error
Duct Top	-50.183 m	61.719 m	243.102
Duct Base	-30.858 m	48.545 m	225.674
Trapping Layer Base	-30.264 m	51.689 m	233.139
Duct Strength	2.117 M-units	4.388 M-units	7.929

IV. RESULTS AND DISCUSSIONS

In this section, we initially will discuss what was found when comparing the FLIP/ RVSR and FLIPI/RVSRI soundings with the ERA5 sounding data. Next, we will analyze the climatology of ducting conditions in the Southern California region and examine trends from year to year and season to season.

A. EVALUATION OF ERA5 ELEVATED DUCT CHARACTERIZATION

After comparing the interpolated soundings to the original soundings, as shown in the previous section, we next compared the ERA5 model data set to both types of soundings for the FLIP and RVSR locations. Figure 7 and Table 3 show the comparison of the FLIP soundings with the ERA5 soundings. The sub-plots of Figure 7 show the duct top and base heights (a and b), trapping layer base height (c), and ducting strength (d) from both the FLIP soundings and the ERA5 soundings. The ERA5 tends to preserve the main features of the ducts and trapping layers fairly well, but there are some key errors to point out. Plot (a) shows that ERA5 performs fairly well at modeling the observed FLIP duct top height for ducts below about 500 m, but it consistently underpredicts the duct top height for ducts above about 500m. The very high degree of scatter in Plot (b) shows that ERA5 has low skill in predicting the duct base height, while Plot (c) demonstrates better skill in predicting the trapping layer base height. Plot (d) shows that ERA5 consistently underpredicts the duct strength. Plots b) and c) also show that with regards to ducting and trapping layer base height, a significant number of cases have ERA5 heights greater than zero when the observation sounding base heights are zero. This also happens in the inverse where the ERA5 data have a base height of zero and the observations have a base height greater than zero.

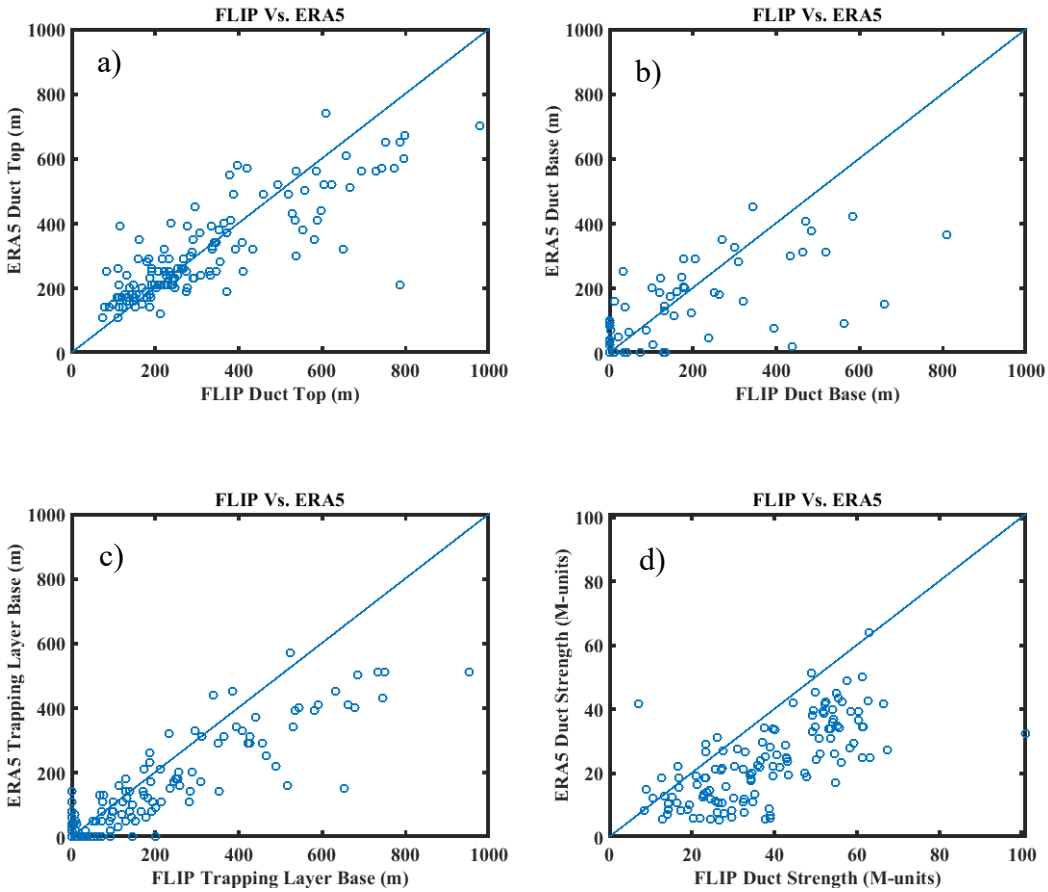

The heights of the duct tops (a), duct bases (b), and the trapping layer bases (c) are shown as well as the duct strengths (d).

Figure 7. Characteristics of the FLIP soundings against the ERA5 soundings.

Table 3. Mean difference, absolute mean difference, and root mean square error between the FLIP soundings and the ERA5 soundings of the duct top, duct base, trapping layer base, and duct strength.

	Mean Difference	Absolute Mean Difference	Root Mean Square Error
Duct Top	22.480 m	101.055 m	196.080
Duct Base	32.735 m	68.326 m	192.191
Trapping Layer Base	69.537 m	98.984 m	200.841
Duct Strength	14.072 M-units	15.475 M-units	15.811

Figure 8 and Table 4 show the comparison of the FLIPI soundings with the ERA5 soundings. The sub-plots of Figure 8 show the duct base and top heights (a and b), trapping

layer base height (c), and ducting strength (d) from both the FLIPI soundings and the ERA5 soundings. Similar to the results shown in Figure 7, the ERA5 tends to preserve the main features of the ducts and trapping layers fairly well.

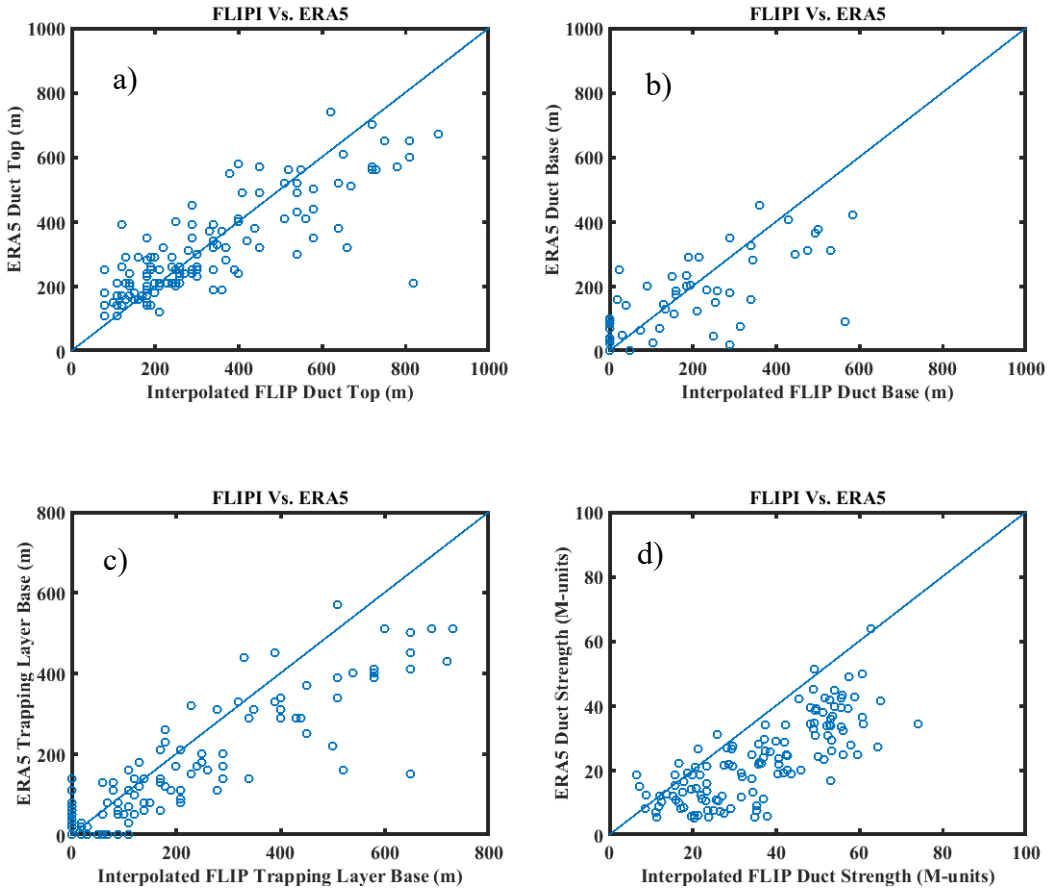

The heights of the duct tops (a), duct bases (b), and the trapping layer bases (c) are shown as well as the duct strengths (d).

Figure 8. Characteristics of the FLIPI soundings against the ERA5 soundings.

Table 4 shows that the duct and trapping layer characterizations from the ERA5 have smaller errors for every statistic computed when compared to the interpolated FLIPI soundings than with the original FLIP data. The absolute mean difference in the height field have improved by 13m for the duct tops, 29m for the duct bases, and 25m for the trapping layer bases. The absolute mean difference in duct strength has also improved 2

M-units. Overall, by interpolating the FLIP data, we can see some significant improvements when compared to the ERA5 data set.

Table 4. Mean difference, absolute mean difference, and root mean square error between the FLIPI soundings and the ERA5 soundings of the duct top, duct base, trapping layer base, and duct strength.

	Mean Difference	**Absolute Mean Difference**	**Root Mean Square Error**
Duct Top	5.758 m	88.333 m	110.739
Duct Base	7.235 m	39.432 m	72.647
Trapping Layer Base	41.667 m	73.333 m	94.569
Duct Strength	12.243 M-units	13.885 M-units	14.142

Figure 9 and Table 5 plot the sounding data from the RVSR and the ERA5 model data set. The ERA5 model data set preserves the main features, similar to the FLIP and the FLIPI comparison, but on average under-predicts all the height features (plots (a), (b), and (c)). Plot (d) shows that duct strength has much scatter and on average ERA5 underestimates the duct strength. The grouping of the points in Figure 9 are generally closer together when compared to Figure 7, with the exception of duct strength. The effect where the RVSR soundings have a zero meter height in plots (b), and (c) and the ERA5 model data set shows a non-zero value for the same data point appears, similar to the FLIP data.

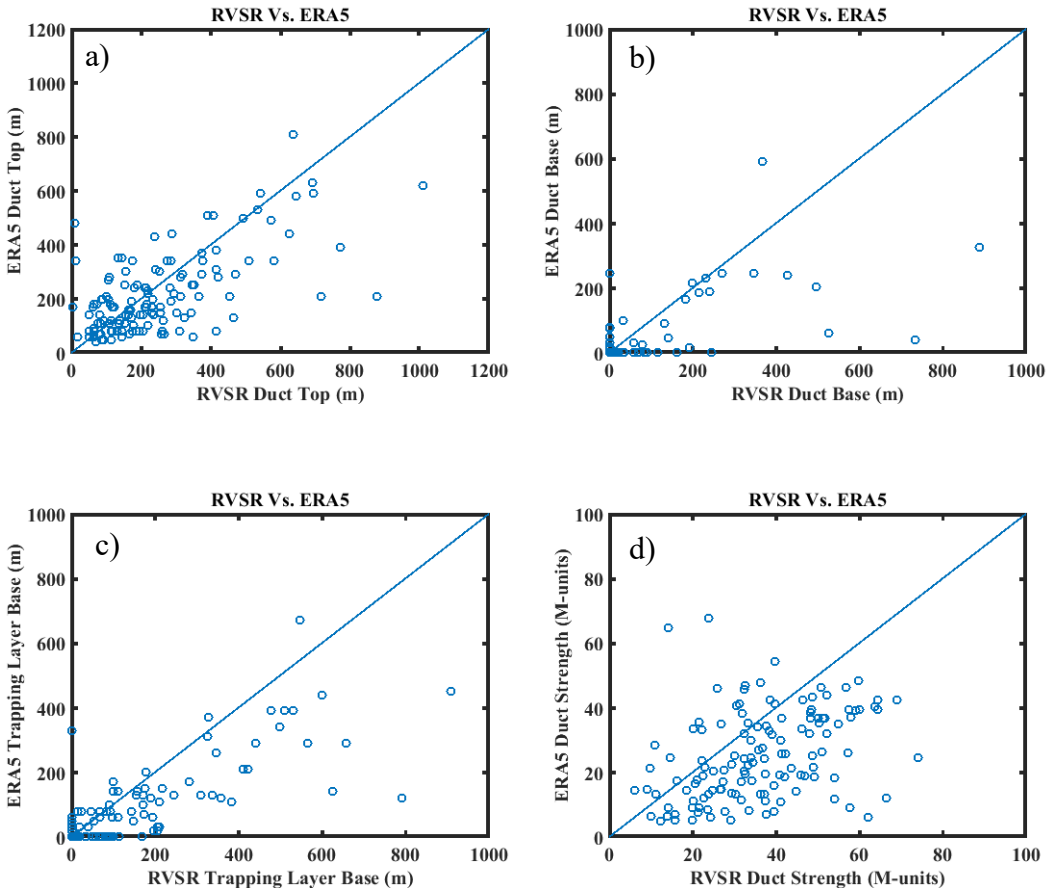

The heights of the duct tops (a), duct bases (b), and the trapping layer bases (c) are shown as well as the duct strengths (d).

Figure 9. Characteristics of the RVSR soundings against the ERA5 soundings.

Table 5 shows that the ERA5 is more accurate in analyzing the duct and trapping layer bases for the RVSR locations than the FLIP location but has similar accuracy for the duct tops and strength. Between the RVSR and FLIP, the ERA5 improves by 34m for the absolute mean difference in duct and trapping layer bases. This is more than likely due to there being more data points to compare the model to as well as more of the RVSR locations being closer to the actual horizontal grid points of the ERA5.

Table 5. Mean difference, absolute mean difference, and root mean square error between the RVSR soundings and the ERA5 soundings of the duct top, duct base, trapping layer base, and duct strength.

	Mean Difference	Absolute Mean Difference	Root Mean Square Error
Duct Top	24.705 m	102.709 m	117.29
Duct Base	22.441 m	34.251 m	82.510
Trapping Layer Base	44.905 m	64.729 m	96.480
Duct Strength	8.539 M-units	16.727 M-units	16.723

Figure 10 and Table 6 show the comparison between RVSRI and ERA5 sounding data. As expected, the ERA5 data more accurately portrays the ducting conditions of the interpolated data as opposed to the original data, however, the improvement is not as drastic as it was with the FLIP data. Table 6 shows absolute mean height improvements of 2m and 7m for duct top and duct base heights, 7m for the trapping layer base heights, and 1 M-units for duct strength.

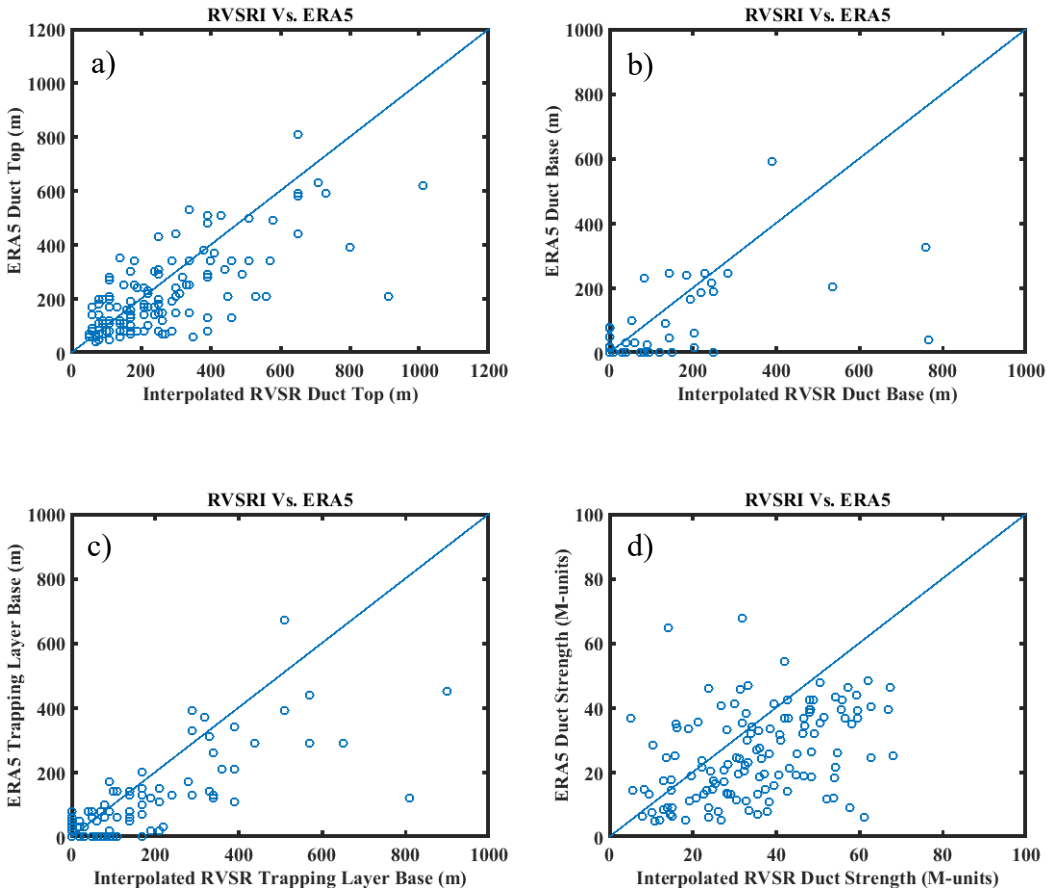

The heights of the duct tops (a), duct bases (b), and the trapping layer bases (c) are shown as well as the duct strengths (d).

Figure 10. Characteristics of the RVSRI soundings against the ERA5 soundings.

Table 6. Mean difference, absolute mean difference, and root mean square error between the RVSRI soundings and the ERA5 soundings of the duct top, duct base, trapping layer base, and duct strength.

	Mean Difference	Absolute Mean Difference	Root Mean Square Error
Duct Top	33.521 m	100.282 m	111.918
Duct Base	16.373 m	27.923 m	71.750
Trapping Layer Base	39.788 m	57.535 m	87.096
Duct Strength	7.011 M-units	15.627 M-units	15.464

B. CLIMATOLOGY OF ELEVATED DUCTS IN THE SOUTHERN CALIFORNIA REGION

To analyze the Southern California ducting climate during the period from 2011 to the end of 2020, we perform analyses of both spatial and temporal variations. We first look at how the ducting conditions vary spatially over the Southern California region and also how they vary temporally by season within this nine-year time period. We grouped each year by four seasons, Winter (December, January, February (DJF)); Spring (March, April, May (MAM)); Summer (June, July, August (JJA)); Fall (September, October, November (SON)). Plots (a), (b), (c), and (d) of the regional color-contoured map views correspond to DJF, MAM, JJA, and SON respectively. Plot (a) of Figure 11 shows the southern California bight region that was analyzed in this study. Plot (a) also shows the ERA5 grid point locations, an example of the spatial distribution of upper-air duct types in the region. Plot (b) of Figure 11 shows geographical points of interest in our analyses as we looked at variations in different variables and ducting conditions. The location of the FLIP (blue dot) and Point Mugu (red dot) from the CASPER-West project are show as well as a Southwest (SW) Point over the ocean (cyan dot) and a Northeast (NE) Point over the land (magenta dot).

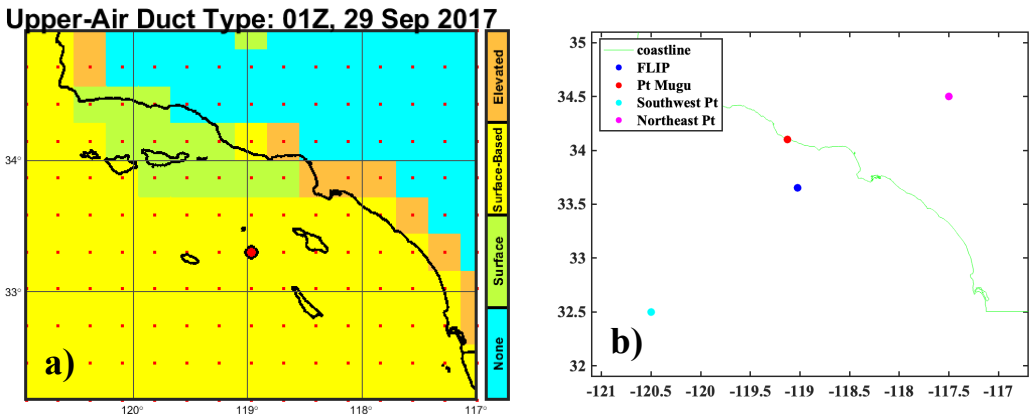

Plot (a) shows the region of study as well as the horizontal grid points for the ERA5 data set. This particular graph shows the type duct present over the region at each ERA5 grid point and plot (b) is the same domain as plot (a) but with points of interest highlighted

Figure 11. Domain of the study and points of interest

Figure 12 shows the average surface temperature for the four seasons. In plot (a) for the DJF season, the maximum average surface temperatures are greater than 288K over the ocean. The 286K contour roughly follows the coastline and the minimum average surface temperature is recorded over land as less than 280K. In plot (b) for the MAM season, the maximum average surface temperature is now located over land close to the NE Point at greater than 294K and the minimum is now located over the ocean of less than 286K, right of the Northwest coastline. The contour following the coastline is no longer present and the temperature contours now intersect the coastline semi-perpendicularly. Plot (c) for the JJA season, shows the greatest surface temperature averages of greater than 305K near the NE Point and less than 290K over the ocean, while the 295K contour follows the coastline. Finally in plot (d) for the SON season, the average maximum has decreased from the Summer to greater than 294K just West of Point Mugu, and the minimum has also decreased to less than 289K near the NW Point.

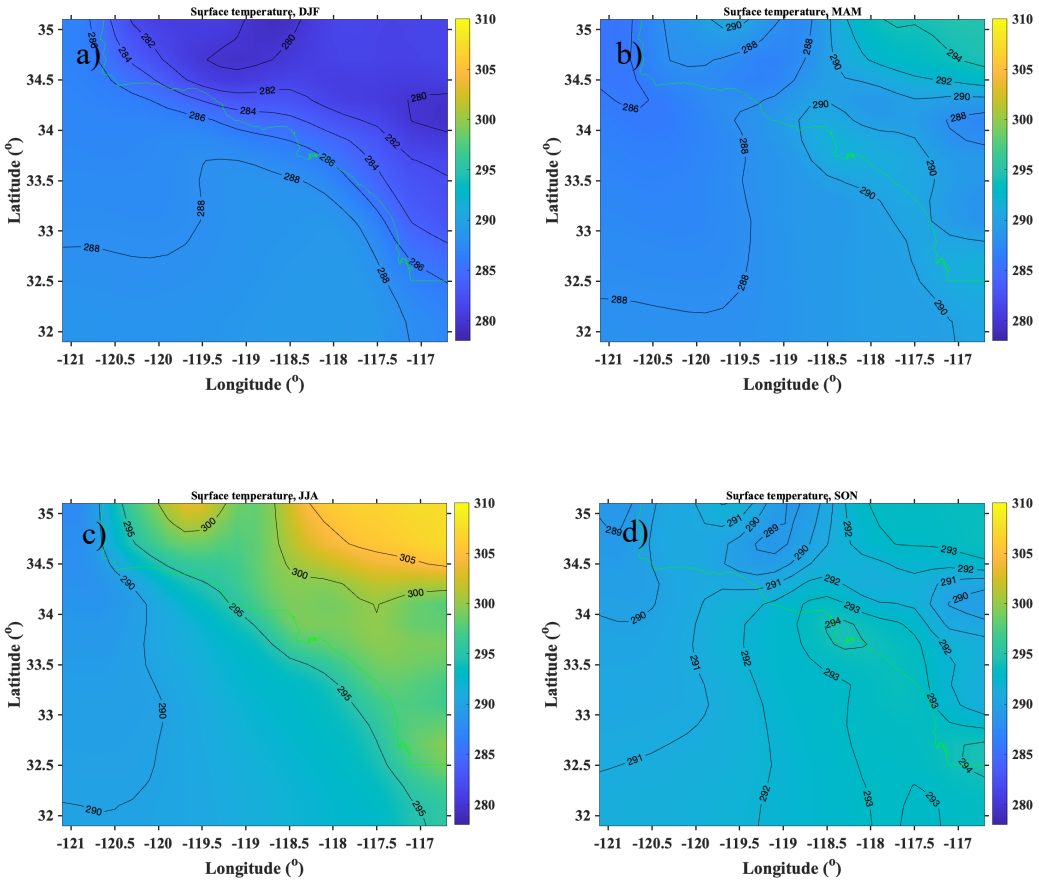

Figure 12. Average surface temperatures (K) in the Southern California region at DJF (a), MAM (b), JJA (c) and SON (d)

Similar to the average surface temperature plots, Figure 13 shows the 10m temperature for each season. Plot (a) is similar to plot (a) from Figure 12 in that the 286K countor line follows the coastline. The maximum average temperature is only greater than 286K and is nearly uniform over the ocean, while the average minimum temperature is less than 282K over land. Plot (b) is also similar to plot (b) from Figure 12, with slightly decreased temperatures. Maximums of over 290K are located over land close to the NE Point while the minimum of 286K is now located over the ocean. The 292K contour follows the coastline in plot (c) with a maximum of greater than 300K located near the NE Point while the average minimum temperatures are still located over the ocean with less than 288K. Finally in plot (d), we see maximum average temperatures of greather than 291K over land and less then 289K over the ocean.

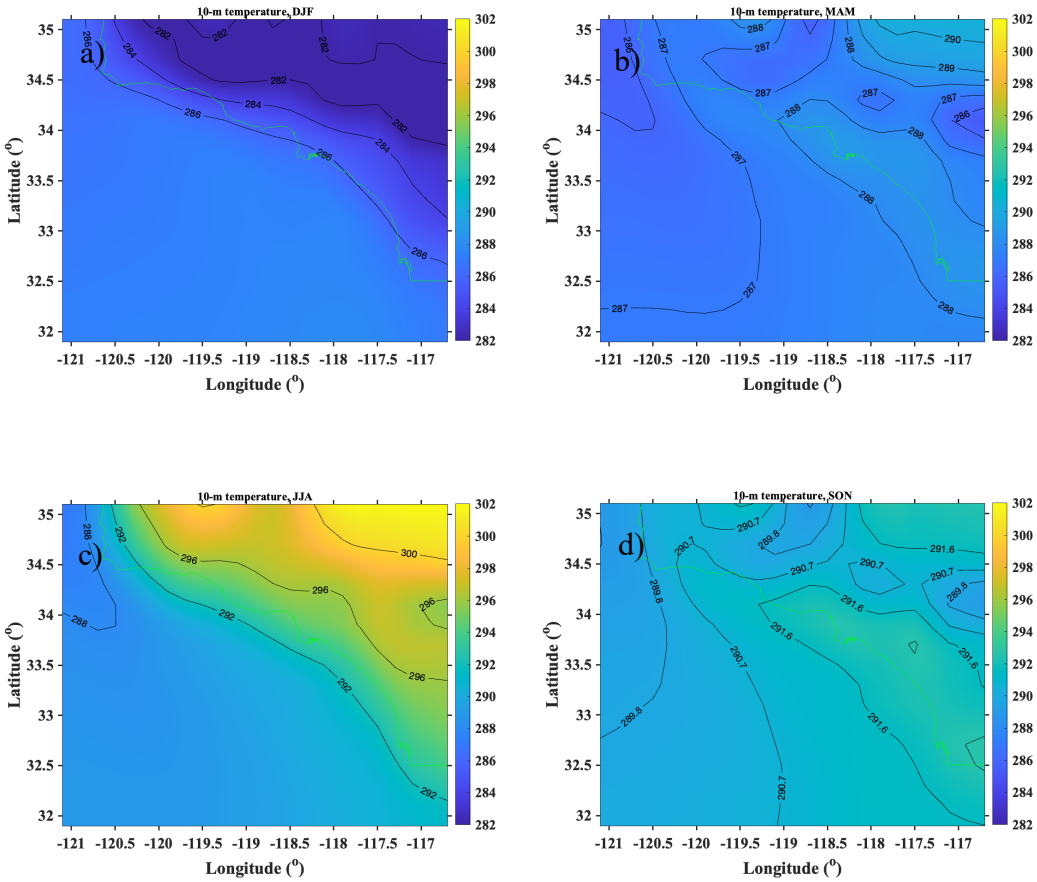

Figure 13. Average 10-m temperatures (K) in the Southern California region at DJF (a), MAM (b), MAM (c) and SON (d)

Figure 14 shows the average air (10 m) and surface temperature differences (ASTDs) for each season. This is a good measure of where stable (positive ASTD values) and unstable (negative ASTD values) conditions occur. Plot (a) shows negative ASTD values over the ocean (less than -0.7 K) while positive values occur over land (greater than 1.4K). The zero contour follows the coastline, acting as a rough "boundary" between the stable and unstable air masses. Plot (b) does not show as uniform differences between land and ocean regions as seen in plot (a). Only a few areas have greater than zero ASTD values, which are located over the ocean, while the rest of the ocean and land areas have negative ASTD values. The strongest unstable conditions (negative ASTD values) are located near the NE Point, with values less than -4 K. Plot (c) for the JJA season exhibits the largest ASTD values out of the four plots. The lowest ASTD values of greater than -2 K are mainly

located over the ocean, while the highest temperature differences of less than -6 K are located near the NE Point. Finally, plot (d) for the SON season shows that ASTD values of less than -1.4 K occur both over the ocean and over land near the NE Point while greater than 0.7 K ASTD values occur only over land.

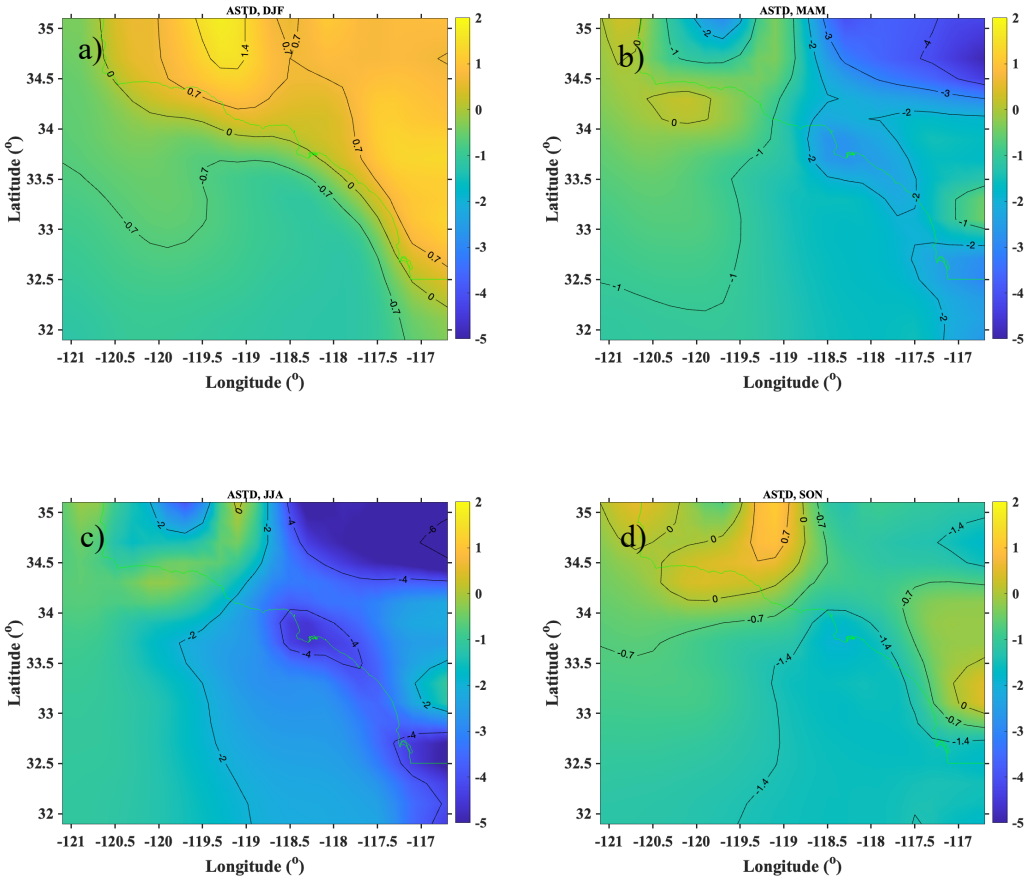

Figure 14. Average air and surface temperatures (K) differences in the Southern California region at DJF (a), MAM (b), JJA (c) and SON (d)

Figure 15 shows the time series for average surface temperatures (a), average 10 m temperatures (b), and difference of these two temperature averages (c). Each plot shows the different temperature for each point of intrest over the 9 years. It comes as no surprise that the further a point is from the ocean, the greater difference in the temperature maximas and minimas. The NE point, being located so far inland, has the greatest varitions overall and season to season with the greatest and lowest average temperature occuring in 2017.

The lowest variations are observed at the SW Pt as the ocean temperature doesn't have great variation from season to season. Plot (c) shows that the SW Point and the FLIP location stay relativly unstable for the entire time period while the NE Point and Point Mugu only have unstable air during the warmer months and stable conditions during the colder months.

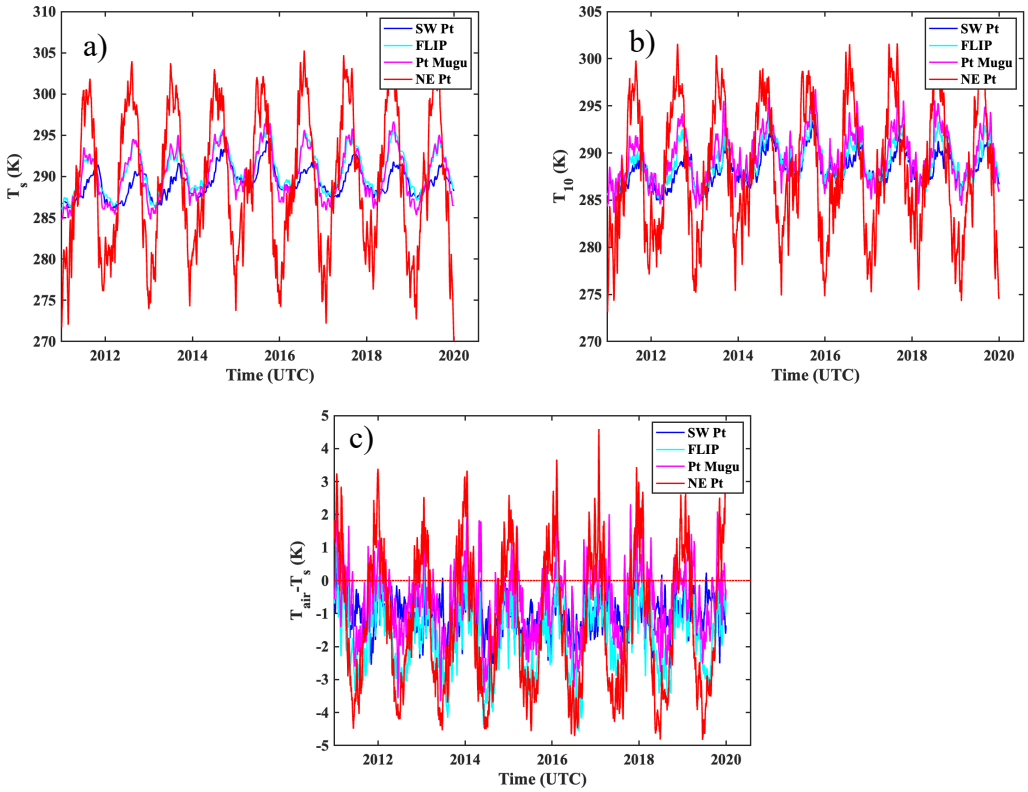

The average surface temperatures (a), average 10-m temperatures (b), and difference of air and surface temperatures (c) are shown.

Figure 15. Time series at the SW Point (blue line), FLIP (cyan line), Point Mugu (pink line), and NE Point (red line)

Figure 16 shows the average of wind speeds for the four seasons over the 9 years. The reason we wanted to plot wind speed is because it's a driving force of temperature changes. The greatest wind speeds in all four plots occur over the ocean while the lowest wind speeds occur over the land. This is most likely due to the increased friction over land than over the ocean. Other than the maximum wind speed of greater than 8 m/s observed

in plot (b), the seasons are very similar when it comes to wind speed. Wind speeds increase as you get further away from the coastline, the 3 or 4 m/s contour tends to follow the coastline, and the coast has wind speeds of 2 m/s or less and increases as you move further inland.

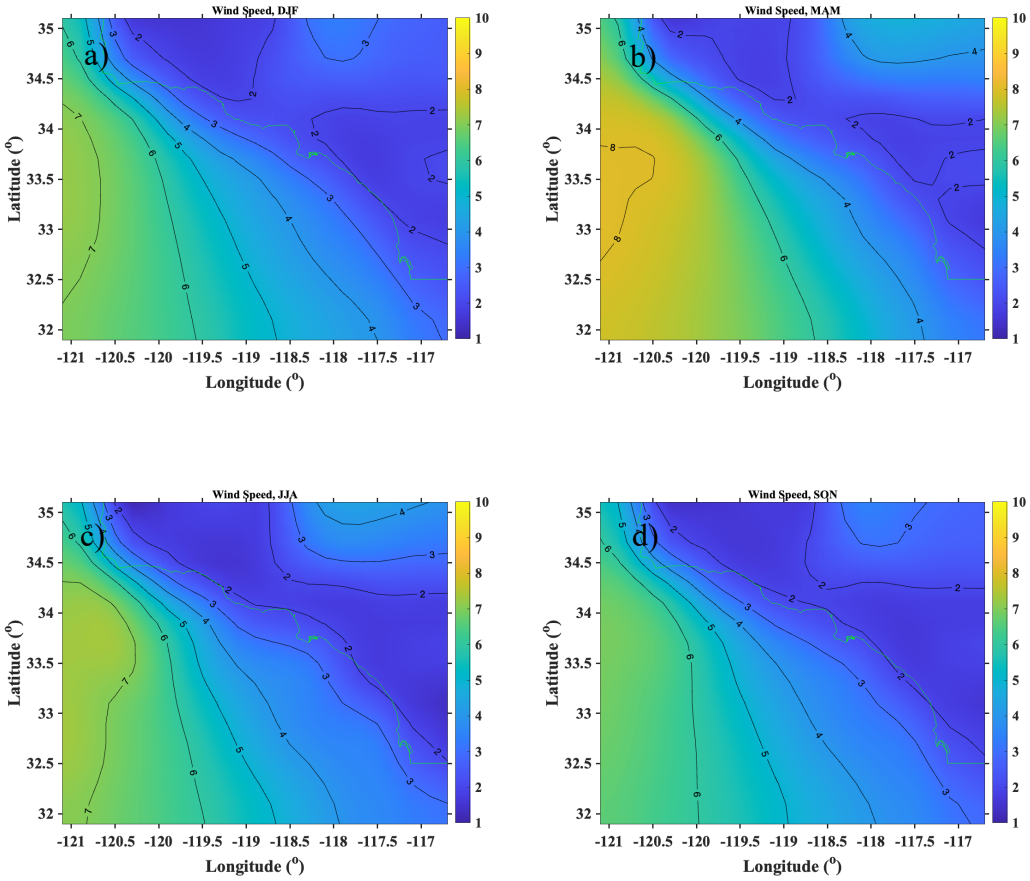

Figure 16. Average wind speed (m/s) in the Southern California region at DJF(a), MAM (b), JJA (c) and SON(d)

Figure 17 shows the average specific humidity over the four seasons. Higher specific humidity values correlate to stronger duct strengths in that region and vice versa for lower specific humidity values. Plot (a) shows values of greater than 7 g/kg over the ocean with the 6 g/kg contour line generally following the coastline and values of less than 4 g/kg located by the NE Pt and the surrounding land around the point. Plot (b) has similar specific humidity patterns but generally slightly higher values. Close to the FLIP location,

values of greater than 8 g/kg occur, while the 7 g/kg contour line follows the coastline, and the area around the NE Point has values of less than 5 g/kg. Plot (c) has the highest values of specific humidity observed in the four plots with a greater than 11 g/kg region off of the Southern coastline. The majority of the ocean is in a region between 9 and 11 g/kg while the area around the NE Point has values less than 7 g/kg. Finally, plot (d) shows slightly lower values than plot (c), with the Southeast region of the ocean now down to greater than 10 g/kg with the 9 g/kg contour line following the coastline, and the region around the NE Point now down to less than 5 g/kg.

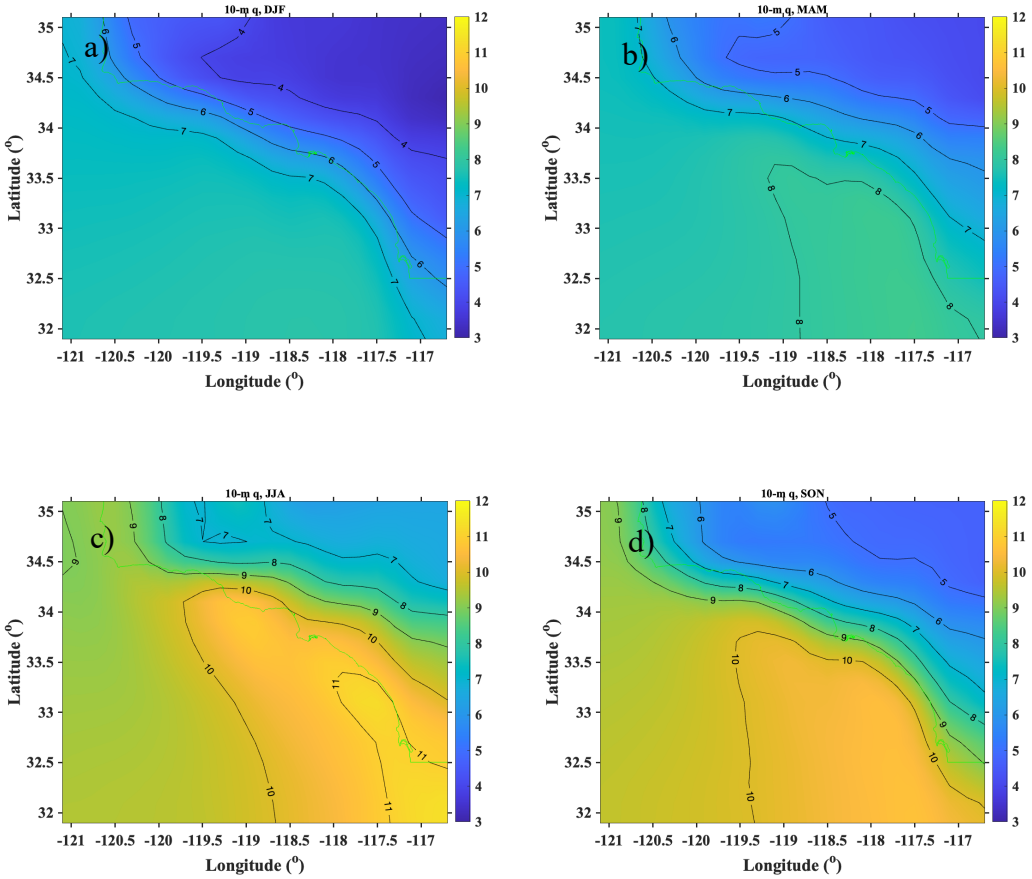

Figure 17. Average specific humidity (g/kg) in the Southern California region at DJF (a), MAM (b), JJA (c) and SON (d)

Figure 18 shows the time series of the wind speed (a) and the specific humidity (b). As seen in Figure 16, higher wind speeds occur at locations further from land, and higher

wind speeds also occur during the warmer months and lower wind speeds occur in the colder months. With regards to plot (b), the SW Point, FLIP location, and Point Mugu have similar trends in specific humidity values. Higher values are observed during SON and the lower values observed during DJF. We observe the highest values of specific humidity during the beginning of 2016. As expected, the NE Point exhibits the lowest values of specfic humidity, since it is the farthest point from the ocean. The NE Point follows the same trends as the other points, with higher values of specific humidity occuring during SON and lower values occuring during DJF, but with much lower values than the other points and smaller variations. The values of the NE Point only come close to the other points specific humidity values during SON and then tends to drop off at the beginning of each new year.

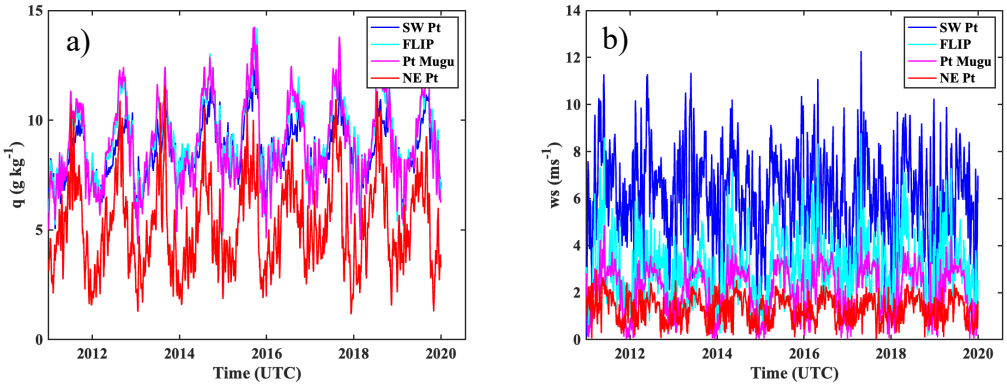

Shown are the average specific humidities (a) and the average wind speeds (b).

Figure 18. Time series at the SW Point (blue line), FLIP (cyan line), Point Mugu (pink line), and NEPoint (red line)

Figure 19 shows the trapping layer base heights for the four seasons. Plot (a) for the DJF winter season shows higher trapping layer base heights occuring over the ocean, with heights of greater than 300 meters occuring around the SW Point. The base height decreases as you approach the coastline with no areas over land reaching above 100 m, and with the majority of the land areas having base heights close to 0 m. Plot (b) shows an increase in base height across the majority of the domain. The highest base heights occur again close to the SW Point, with heights greater than 400 m, and the lowest heights

occuring over land and a small portion over the ocean, with values less than 100 m. There is an area of higher base heights occuring over land in the Los Angeles area of greater than 200 m, which increases in the warmer months. In plot (c), we again observe base heights of greater than 400 m located by the SW Point and we also see that the base height over the Los Angeles area is also greater than 400 m Further South of Los Angeles, there is another area over land of high base heights around San Diego with values greater than 300 m observed. An area with base heights less than 100 m is located over land, but the area has decreased significantly from the previous plot. Plot (d) is very similar to plot (b) with contour strength and location. The main difference between the two plots is that near the SW Point the base hight values are roughly 300 m instead of around 400 m, and the greater than 200 m maxima area around Los Angeles is smaller in size than the area in plot (b).

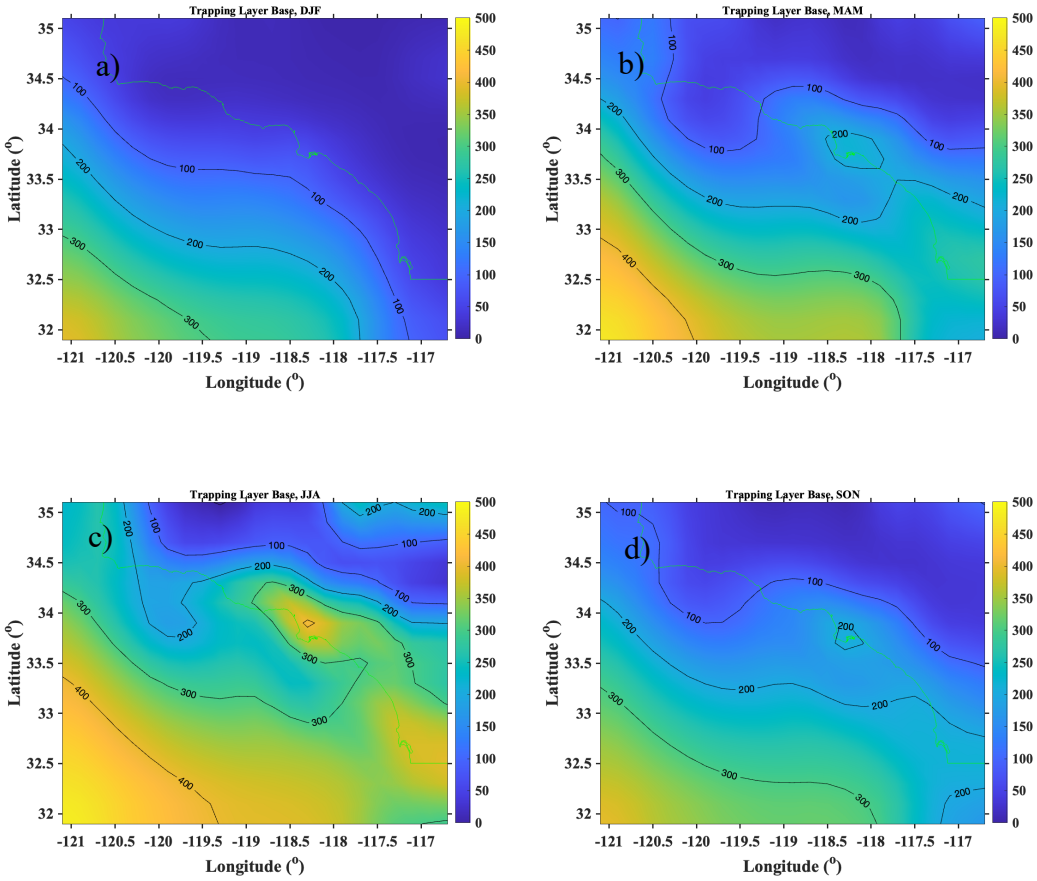

Figure 19. Average trapping layer base (m) in the Southern California region at DJF (a), MAM (b), JJA (c) and SON (d)

Figure 20 shows the percentage of duct occurrence for the different seasons. This figure shows that the warmer the season, the greater chance there is for ducting formation. In plot (a) for the DJF season, there is a duct occurrence of between 87% and 90% occurring over most of the ocean areas, and a minimum of less than 78% duct occurrence over land areas. In plot (b) for the MAM season, the maximum duct occurrence decreases to 88% over the ocean and the minimum occurrence also decreases to 76% over land. Plot (c) for the JJA months shows the greatest increase for the maximum duct occurrence of greater than 95%, which occurs over the ocean, and a minimum of less than 80% occurrence over the land. Finally, plot (d) for the SON months shows the largest area for above 90% occurrence of ducting formation over the ocean following the coastline. The minimum frequency of duct occurrence is similar to plot (c) with a less than 80% occurrence over land.

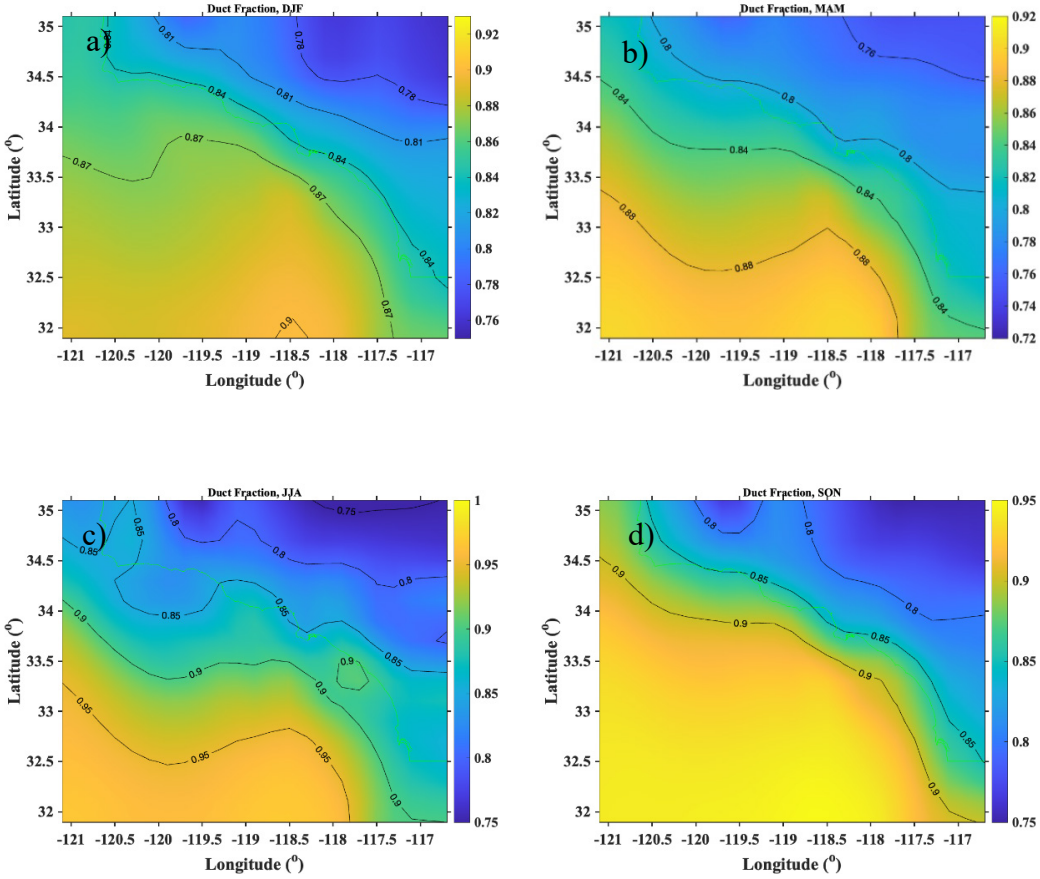

Figure 20. Percentage of duct formation in the Southern California Region for DJF (a), MAM (b), JJA(c), and SON (d)

Figure 21 shows the average height of the duct tops in the Southern California Region. This figure follows similar patterns as the duct bases, but the patterns are slightly more organized and less chaotic. In plot (a) for the winter season, the duct top heights over the ocean increase with distance from the coastline, with a height maxima of greater than 500m located near the SW Point. The 100m contour roughly follows the coastline, and duct top heights over the land are relatively uniform, with heights less than 100 m. In plot (b) for the spring season, the height maxima around the SW Point is greater than 500m. There is also a duct top height maxima of greater than 300m located over Los Angeles. The area of the height minimums has decreased to less than 100m and is only located over land now. In plot (c) for the summer months, the local height maxima is greater than 600m, located in the southwest corner of our domain, and a maxima of greater than 500m occurs over Los Angeles. There are only small sections in plot (c) with heights less than 100m heights occurring over land. Finally, for plot (d) portraying the autumn months, the maxima height has decreased to greater than 500m around the SW Point and the minimum over land has also decreased to 100m. The contours also roughly follow the coastline, similar to plot (a) for the winter months.

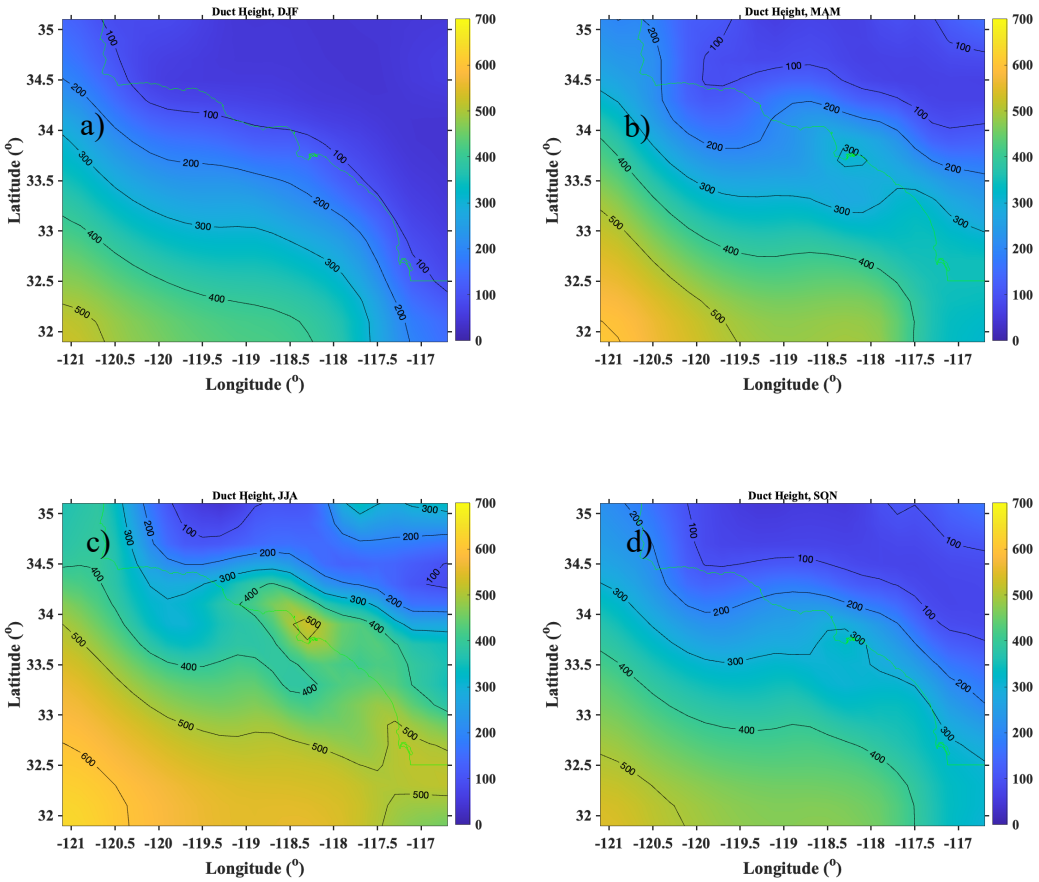

Figure 21. Average height (m) of the duct tops in the Southern California Region for DJF (a), MAM (b), JJA(c), and SON (d)

Figure 22 shows the average height of the duct base by season. In plot (a) for the winter months, the maximum height is greater than 210m around the SW Point, while the minima is located over land and is less than 70m. The 70m contour seems to follow the coastline but only for plot (a). In plot (b) for the spring months, the maximum duct base height increases to above 320m, and has the same location as plot (a). The minimum increases slightly to less than 80m but it covers a smaller area than in plot (a). Over Los Angeles, there is an area of greater than 160m as well. In plot (c) for the summer months, there is actually a decrease in the maximum height of greater than 280m but it occurs in broader areas. There is still a maximum by the SW Point, but there are also two more maximums located over land, one over Los Angeles and another maximum further south over San Diego. The minimum height has stayed the same compared to the other plots, less

than 70m, but the area which it covers is much smaller. The minimum occurs only over land now, and around the NE Point of our plot is "sandwiched" in-between higher duct heights. Finally, plot (d) for the autumn months has similar locations of the maximums and minimums as plot (b), but they are not as high, with maxima of greater than 180m by the SW Point and maximums greater than 120m located over Los Angeles and San Diego. The minimum area has increased from plot (c) and has decreased in height slightly, with less than 60m in the area.

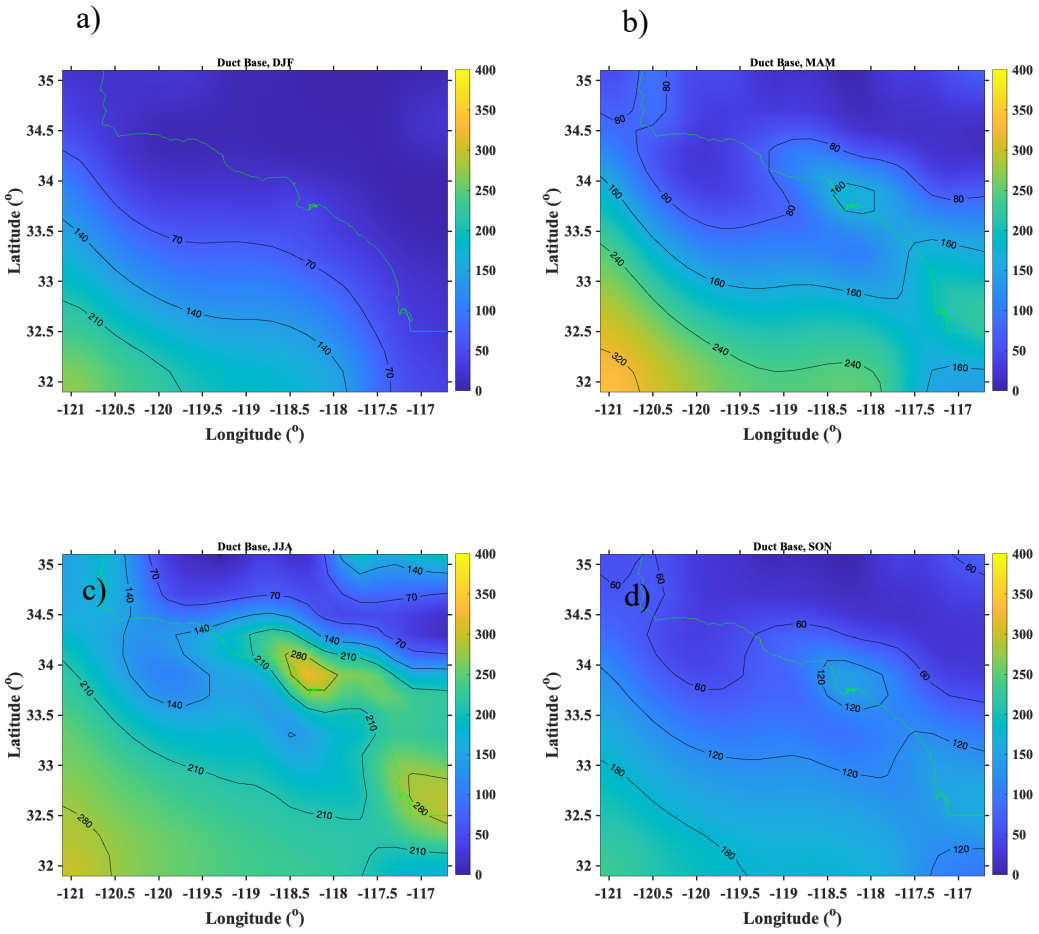

Figure 22. Average height (m) of the duct bases in the Southern California Region for DJF (a), MAM (b), JJA (c), and SON (d)

Figure 23 shows the average duct strength for the four seasons. In all cases, weaker ducts generally occur over land areas, due to the lower humidity in the layer near the surface, which leads to smaller humidity and refractivity decreases within the duct. In plot

(a) for the winter months, the average maximum duct strength occurs over the ocean, with a maximum of greater than 16 M-units, while the minimum averages occur over the land with less than 4 M-units. In plot (b) for the spring months, the maximum decreases to a small area over the ocean with a greater than 15 M-units while the minimum increases to less than 6 M-units. In plot (c), the maximum increases in area and magnitude over the ocean at 16 M-units and the minimum also increases over land to less than 8 M-units. Finally, plot (d) shows the greatest maximum strength of greater than 20 M-units located over the ocean while the minimum decreases to less than 5 M-units over land.

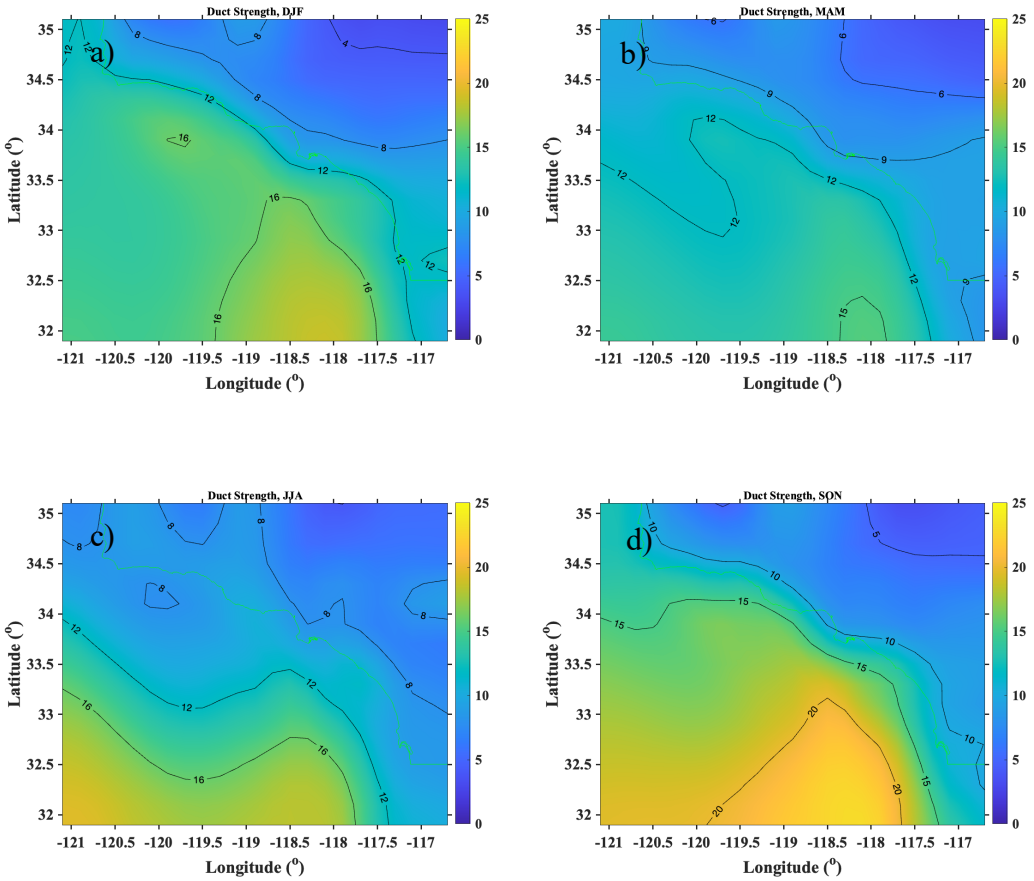

Figure 23. Average duct strength (M-units) in the Southern California Region for DJF (a), MAM(b), JJA (c), and SON (d)

Figure 24 is a time series of the mean duct and trapping layer characteristics. Plots (a), (b), and (c) show lower heights occurring in the colder months and higher heights

occurring in the warmer months. Maximums heights occurring in mid-2015, early 2016, and late 2019 while minimums heights occurring at the beginning of 2014 and 2018. Similar to the spatial plots, the higher heights are correlated with where each point is in relation to the ocean and vice versa with the lower heights occurring over land. Plot (d) shows that the SW Point, FLIP and Point Mugu duct strength values stay consistent with each other throughout the time frame, with the SW Point having the strongest duct with only a few months where the FLIP location had stronger ducts.

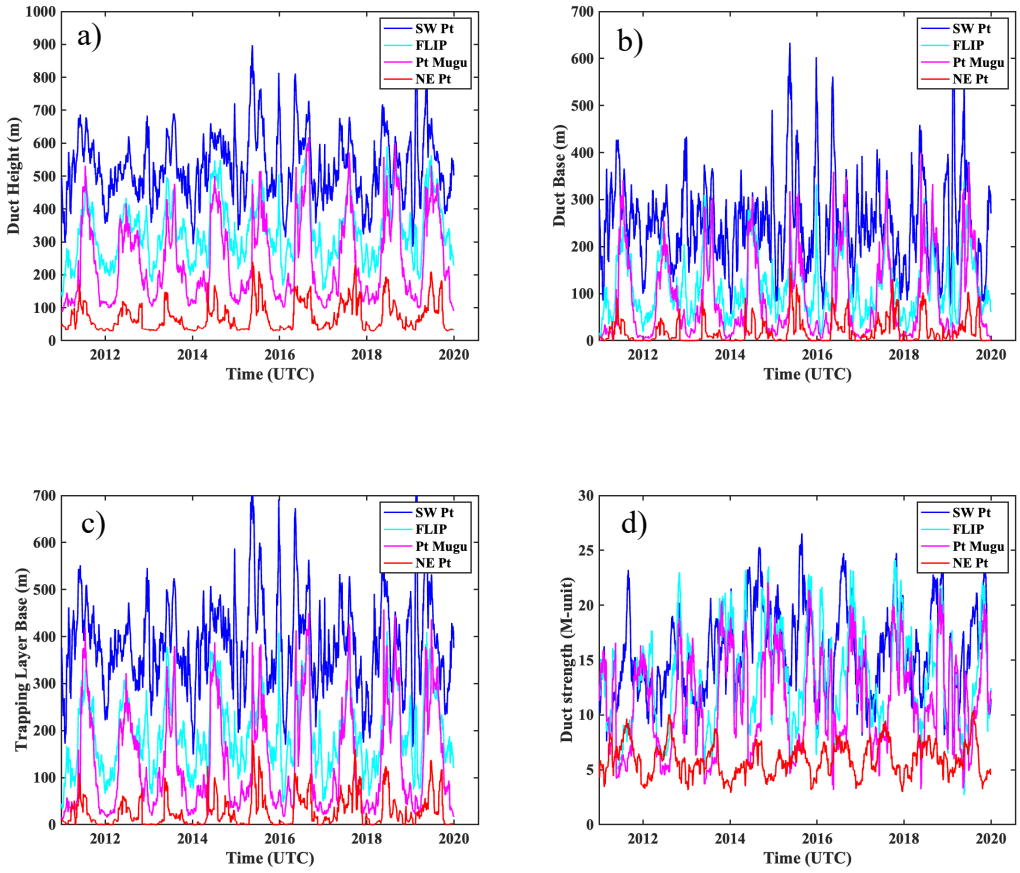

Shown are the average duct tops (a), the average duct bases (b), average trapping layer bases (c), and average duct strengths (d).

Figure 24. Time series at the SW Point (blue line), FLIP (cyan line), Point Mugu (pink line), and NE Point (red line)

THIS PAGE INTENTIONALLY LEFT BLANK

V. CONCLUSIONS

The Air Force and the Navy depend on EM wave propagation within the atmosphere for detecting and tracking targets and guiding munitions, as well as for communications. Understanding how those EM waves propagate in the past, present, and future are crucial to forecasting EM wave propagation in a changing climate. Utilizing model data sets to analyze past and future climate for EM wave propagation is critical for DOD operations to run smoothly and effectively.

This thesis first focused on evaluating the ERA5 model data set with the CASPER-West Project. We found that even with a coarse horizontal grid resolution, the ERA5 tended to predict the main observed features of the trapping and ducting layer characteristics reasonably well. The heights of the ducts and trapping layers were on average between 34m and 104m when comparing against non-interpolated data and 27m and 100m when comparing against interpolated data with only a few extreme outliers. With regards to duct strength, a difference of 15 to 16 M-units on average and 13 to 15 M-units on average when compared to non-interpolated and interpolated sounding data, respectively. These ERA5 errors are small enough to justify using that database to make informed decisions on what past ducting conditions have been and what they may be in the future.

The second focus was to evaluate the ducting and trapping layer characteristics in Southern California from 2011 to 2020. What we observed is a small year-to-year variation in the ducting characteristics, with the exception of the summer of 2015 having higher values than the rest of the data set. We were able to identify some trends in the ducting characteristics with regards to how close a location is to the coastline and from season to season. Generally, the further away an ocean location is from land, the higher and stronger ducts will be and the more likely they are to occur. The SW Point., FLIP, and Point Mugu saw similar values in ducting characteristics while the NE Point. saw much lower values in those same characteristics. This is due to lower specific humidity levels over land as well as temperatures fluctuating more over land then over the ocean. The ducting characteristics decreased as we went from warmer months to colder months and increased as we went from colder months to warmer months. We also observed that human

infrastructure has an impact in the height of the duct. The result of increased instability over the Los Angeles and San Diego areas was to also increase the boundary layer height which, in turn, increased the height of the duct and trapping layer heights.

This thesis only scratched the surface in ducting climatology and a lot more can be done in the future. First, utilizing a longer data set would allow us to get a more accurate climatology of the region we are focused on. Secondly, taking the diurnal and night average instead of just the day average would allow a better comparison between the averages of values over land and over the ocean. The difference between the locations would not be as drastic and we could see a true difference between ducts over the land versus over the ocean. Third, is analyzing the different locations and their relation to the ocean and to human infrastructure. We were able to identify Los Angeles and San Diego having an impact on duct heights but to ensure it was those cities impacting the duct height rather than just model error, we would want to analyze other big and small cities that are near and far from water areas to get a better idea what impacts the cities play in affecting duct height and how big does a city need to be before the impacts are translated to duct heights.

LIST OF REFERENCES

Bean, B. R., and Dutton, E. J., 1966: *Radio Meteorology*, National Bureau of Standards, 435 pp.

Hersbach, H., and Coauthors, 2020: The ERA5 global reanalysis, *Quarterly Journal of the Royal Meteorological Society,* **146,1999-2049,** https://doi.org/10.1002/qj.3803

LeMay Center for Doctrine, 2019: Air Force Doctrine Publication (AFDP) 3–51, Electromagnetic Warfare and Electromagnetic Spectrum Operations. Accessed 15 July 2022, https://www.doctrine.af.mil/Portals/61/documents/AFDP_3-51/3-51-D01-EW-EMSO-Introduction.pdf

Lopez, P., 2009: A 5-yr 40-km-Resolution Global Climatology of Superrefraction for Ground-Based Weather Radars, *American Meteorological Society,* **48,** 89–110, https://doi.org/10.1175/2008JAMC1961.1

Pörtner, H.-O., and Coauthors, 2022: Climate Change 2022: Impacts, Adaptation and Vulnerability. Contribution of Working Group II to the Sixth Assessment Report of the Intergovernmental Panel on Climate Change, 3056 pp., https://doi.org/10.1017/9781009325844.

Turton, J.D., Bennetts, D.A., and Farmer, S.F.G., 1988: An introduction to radio ducting, *Meteorological Magazine,* **117,** 245–254

von Engeln, A. and Teixeria, J., 2004: A ducting climatology derived from the European Centre for Medium-Range Weather Forecasts global analysis fields, *Journal of Geophysical Research: Atmospheres,* **109**, 148–227, https://doi.org/10.1029/2003JD004380

Wang, Q., and Coauthors, 2018: CASPER: Coupled Air-Sea Processes and Electromagnetic Ducting Research, *American Meteorological Society,* **99,** 11449-1471, https://doi.org/10.1175/BAMS-D-16-0046.1

Wang, Q., and Coauthors, 2019: Sampling Spatial-Temporal Variability of Electromagnetic Propagation in CASPER-West, *2019 13th European Conference on Antennas and Propagation (EuCAP),* Krakow, Poland, 2019, pp. 1–5.

THIS PAGE INTENTIONALLY LEFT BLANK

INITIAL DISTRIBUTION LIST

1. Defense Technical Information Center
   Fort Belvoir, Virginia

2. Dudley Knox Library
   Naval Postgraduate School
   Monterey, California